

# THE COMMUNICATION-HIDING CONJUGATE GRADIENT METHOD WITH DEEP PIPELINES\*

JEFFREY CORNELIS<sup>†</sup>, SIEGFRIED COOLS<sup>†</sup>, AND WIM VANROOSE<sup>†</sup>

**Abstract.** Krylov subspace methods are among the most efficient solvers for large scale linear algebra problems. Nevertheless, classic Krylov subspace algorithms do not scale well on massively parallel hardware due to synchronization bottlenecks. Communication-hiding pipelined Krylov subspace methods offer increased parallel scalability by overlapping the time-consuming global communication phase with computations such as SPMVs, hence reducing the impact of the global synchronization and avoiding processor idling. One of the first published methods in this class is the pipelined Conjugate Gradient method (p-CG). However, on large numbers of processors the communication phase may take much longer than the computation of a single SPMV. This work extends the pipelined CG method to deeper pipelines, denoted as  $p(l)$ -CG, which allows further scaling when the global communication phase is the dominant time-consuming factor. By overlapping the global all-to-all reduction phase in each CG iteration with the next  $l$  SPMVs (deep pipelining), the method hides communication latency behind additional computational work. The  $p(l)$ -CG algorithm is derived from similar principles as the existing  $p(l)$ -GMRES method and by exploiting operator symmetry. The  $p(l)$ -CG method is also compared to other Krylov subspace methods, including the closely related classic CG and D-Lanczos methods and the pipelined CG method by Ghysels et al.. By analyzing the maximal accuracy attainable by the  $p(l)$ -CG method it is shown that the pipelining technique induces a trade-off between performance and numerical stability. A preconditioned version of the algorithm is also proposed and storage requirements and performance estimates are discussed. Experimental results demonstrate the possible performance gains and the attainable accuracy of deeper pipelined CG for solving large scale symmetric linear systems.

**Key words.** Krylov subspace methods, Parallel performance, Global communication, Latency hiding, Conjugate Gradients.

**AMS subject classifications.** 65F10, 65N12, 65G50, 65Y05, 65N22.

**1. Introduction.** Krylov subspace methods [28, 36, 39, 43, 48] are well-known as efficient iterative solvers for large scale linear systems of the general form  $Ax = b$ , where  $A$  is an  $n \times n$  matrix and  $b \in \mathbb{R}^n$ . These iterative algorithms construct a sequence of approximate solutions  $\{x_i\}_i$  with  $x_i \in x_0 + \text{span}\{r_0, Ar_0, A^2r_0, \dots, A^{i-1}r_0\}$ , where  $r_0 = b - Ax_0$  is the initial residual. The Conjugate Gradient (CG) method [33], which allows for the solution of systems with symmetric and positive definite (SPD) matrices  $A$ , is generally considered as the first Krylov subspace method. Driven by the ongoing transition of hardware towards the exascale regime, research on the scalability of Krylov subspace methods on massively parallel architectures has recently (re)gained attention in the scientific computing community [16, 17, 18, 22]. Since for many applications the system operator  $A$  is sparse (e.g. given by a local stencil) and thus rather inexpensive to apply in terms of computational and communication cost, the main bottleneck for efficient parallel execution is typically not the sparse matrix-vector product (SPMV), but the communication overhead due to global reductions in dot product computations and the related global synchronization bottleneck. A dot product of two distributed vectors requires the local computation of the dot product contributions, followed by a global reduction tree of height  $\mathcal{O}(\log(N))$ , where  $N$  is the number of nodes. The explicit synchronization of processes involved in this reduction makes the dot product one of the most time consuming operations in the Krylov subspace algorithm on large parallel hardware.

Over the past decades there have been a variety of scientific efforts to reduce or eliminate the

\*Submitted to the editors on January 29, 2019.

**Funding:** This work was funded by the Research Council of the University of Antwerp under the University Research Fund (BOF) (J. Cornelis) and the Research Foundation Flanders (FWO) under grant 12H4617N (S. Cools).

<sup>†</sup>Applied Mathematics Group, Department of Mathematics and Computer Science, University of Antwerp, Building G, Middelheimlaan 1, 2020 Antwerp, Belgium.

synchronization bottleneck in Krylov subspace methods. The earliest papers on synchronization reduction date back to the late 1980’s and 1990’s [45, 13, 15, 20]. A notable reduction of the number of global synchronization points was introduced by the so-called  $s$ -step methods [8, 10, 9, 5, 4, 35]. Other scalable approaches to Krylov subspace methods include hierarchical [37], enlarged [31] and an iteration fusing [50] Krylov subspace methods. In addition to avoiding communication, research on hiding global communication by overlapping communication with computations can be found in the literature [15, 14, 24, 49, 44, 19]. The current work is situated in the latter branch of research.

Introduced in 2014, the so-called “pipelined” CG method (p-CG) [25] aims at hiding global synchronization latency by overlapping the communication phase in the Krylov subspace algorithm by the application of the SPMV. Hence, idle core time is reduced by simultaneous execution of the time-consuming synchronization phase and independent compute-bound calculations. The reorganization of the algorithm introduces auxiliary variables, resulting in several additional AXPY ( $y \leftarrow \alpha x + y$ ) operations required to recursively compute updates for these variables. Since these are local operations, the extra recursions have no impact on the communication flow of the algorithm. However, they may influence numerical stability, as analyzed by the authors in [12]. Additionally, other error effects (e.g. delayed convergence due to loss of basis orthogonality in finite precision [29, 32, 46, 23, 6], hard faults and soft errors [1], etc.) may affect the convergence of pipelined CG.

The original pipelined CG method performs well on problem/hardware setups where the time to compute the SPMV (plus preconditioner application, when applicable) roughly equals the time spent communicating in the global reduction phase, such that a good overlap can be achieved. In this optimal scenario the time to solution can be reduced by a factor  $3\times$  compared to classic CG on sufficiently large numbers of processors, see [25], Table 1 and Section 5. However, in situations where the global reduction takes significantly longer than one SPMV, the performance gain of p-CG over classic CG may be less pronounced. In heavily communication-bound scenarios, which are typically encountered when solving large-scale problems on HPC hardware, a *deeper pipeline* would be required to overlap the global reduction phase with the computational work of multiple SPMVs.

The concept of deep pipelines was introduced by Ghysels et al. [24] for the Generalized Minimal Residual (GMRES) method. In the current work we extend the notion of deep pipelining to the CG method. Assuming the symmetry of the system matrix  $A$ , we establish theoretical properties that allow to derive the algorithm starting from the pipelined Arnoldi process in the original  $p(l)$ -GMRES algorithm [24]. Subsequently, it is shown that the  $p(l)$ -CG algorithm has several interesting properties compared to  $p(l)$ -GMRES, including shorter recurrences for the basis vectors and the Hessenberg elements and significantly reduced storage requirements. We also indicate limitations of the  $p(l)$ -CG method, in particular in comparison to the (length-one) pipelined CG method [25] which was derived using a notably different framework to the one presented here, see also [11].

Reorganizing a Krylov subspace algorithm into a communication reducing variant typically introduces issues with the numerical stability of the algorithm. In exact arithmetic the pipelined CG method produces a series of iterates identical to the classic CG method. However, in finite precision arithmetic their behavior can differ significantly as local rounding errors may decrease attainable accuracy and induce delayed convergence. The impact of round-off errors on numerical stability of classic CG has been extensively studied [26, 29, 27, 32, 46, 47, 40, 23]. Similar observations have been made for other classes of communication reducing methods, see e.g. [8, 4] for the influence of the  $s$ -step parameter on the numerical stability of communication avoiding methods, and [12, 6] for an overview of the stability analysis of the pipelined Conjugate Gradient method proposed in [25].

The remainder of this work is structured as follows. In Section 2 we introduce the mathematical context and notations of this paper by revisiting the  $p(l)$ -GMRES method. We then show how the

$p(l)$ -Arnoldi process simplifies in the case of a symmetric system matrix  $A$  and derive the  $p(l)$ -CG algorithm with pipelines of general length  $l$ . We also comment on a variant of the algorithm that includes preconditioning. Section 3 gives an overview of some crucial implementation issues and corresponding solutions related to the  $p(l)$ -CG algorithm. This section contributes to a better understanding of key aspects of the method from a performance point of view. Section 4 analyzes the behavior of local rounding errors that stem from the multi-term recurrence relations in  $p(l)$ -CG. We characterize the propagation of local rounding errors throughout the algorithm and discuss the influence of the pipelined length  $l$  and the choice of the auxiliary Krylov basis on the maximal accuracy attainable by  $p(l)$ -CG. The numerical analysis is limited to the effect of local rounding errors on attainable accuracy; a discussion of the loss of orthogonality [29, 32] and consequential delay of convergence in pipelined CG is beyond the scope of this work. Numerical experiments validating the  $p(l)$ -CG method are provided in Section 5. These illustrate the attainable speed-up of deeper pipelines on a distributed multicore hardware setup, but also comment on the possibly reduced attainable accuracy when longer pipelines are used. The paper concludes by presenting a summary of the current work and a short discussion on future research directions in Section 6.

**2. From  $l$ -length pipelined GMRES to  $l$ -length pipelined CG.** We use the classic notation  $V_k = [v_0, \dots, v_{k-1}]$  for the orthonormal basis of the  $k$ -th Krylov subspace  $\mathcal{K}_k(A, v_0)$ . Here the index  $k$  denotes the number of basis vectors  $v_j$  in  $V_k$ , with indices  $j$  ranging from 0 up to  $k-1$ . The length of each basis vector  $v_j$  is the column dimension of the system matrix  $A$ .

**2.1. Brief recapitulation of  $p(l)$ -GMRES.** Let  $V_{i-l+1} := [v_0, v_1, \dots, v_{i-l}]$  be the orthonormal basis for the Krylov subspace  $\mathcal{K}_{i-l+1}(A, v_0)$ . These vectors satisfy the Arnoldi relation  $AV_j = V_{j+1}H_{j+1,j}$  for  $1 \leq j \leq i-l$ , where  $H_{j+1,j}$  is the  $(j+1) \times j$  upper Hessenberg matrix. This translates in vector notation to:

$$(1) \quad v_j = \frac{Av_{j-1} - \sum_{k=0}^{j-1} h_{k,j-1}v_k}{h_{j,j-1}}, \quad 1 \leq j \leq i-l.$$

We define the auxiliary vectors  $Z_{i+1} := [z_0, z_1, \dots, z_{i-l}, z_{i-l+1}, \dots, z_i]$  as

$$(2) \quad z_j := \begin{cases} v_0, & j = 0, \\ P_j(A)v_0, & 0 < j \leq l, \\ P_l(A)v_{j-l}, & j > l, \end{cases} \quad \text{with} \quad P_i(t) := \prod_{j=0}^{i-1} (t - \sigma_j), \quad \text{for } i \leq l,$$

where the polynomials  $P_i(t)$  are defined with shifts  $\sigma_j \in \mathbb{R}$  that will be specified later. The basis  $Z_{i+1}$  can alternatively be defined using three-term recurrences, where we refer to Remark 3 and [24] (Section 4.3) for more details on choosing the basis. Note that for any  $i \geq 0$  the bases  $V_{i+1}$  and  $Z_{i+1}$  span the same Krylov subspace. One has the following recurrence relations for successive  $z_j$ :

$$(3) \quad z_j = \begin{cases} (A - \sigma_{j-1}I)z_{j-1}, & 0 < j \leq l, \\ (Az_{j-1} - \sum_{k=0}^{j-l-1} h_{k,j-l-1}z_{k+l})/h_{j-l,j-l-1}, & l < j \leq i. \end{cases}$$

These recursive relations for the vectors  $z_j$  can be summarized in the Arnoldi-type matrix identity

$$(4) \quad AZ_i = Z_{i+1}B_{i+1,i}, \quad \text{with} \quad B_{i+1,i} = \left( \begin{array}{ccc|ccc} \sigma_0 & & & & & \\ 1 & \ddots & & & & \\ & \ddots & \sigma_{l-1} & & & \\ \hline & & & 1 & & \\ & & & & & H_{i-l+1,i-l} \end{array} \right).$$

**THEOREM 1.** [Ghysels et al. [24]] *Suppose  $k > l$  and let  $V_k$  be an orthonormal basis for the  $k$ -th Krylov subspace  $\mathcal{K}_k(A, v_0)$ . Let  $Z_k$  be a set of vectors defined by (2). Then the identity  $Z_k = V_k G_k$  holds with  $G_k$  an upper triangular  $k \times k$  matrix. The entries of the last column of  $G_k$ , i.e.  $g_{j,k-1} = (z_{k-1}, v_j)$  (with  $j = 0, \dots, k-1$ ), can be computed using the elements of  $G_{k-1}$  and the dot products  $(z_{k-1}, v_j)$  that are available for  $j \leq k-l-1$  and  $(z_{k-1}, z_j)$  for  $k-l-1 < j \leq k-1$ :*

$$(5) \quad g_{j,k-1} = \frac{(z_{k-1}, z_j) - \sum_{m=0}^{j-1} g_{m,j} g_{m,k-1}}{g_{j,j}} \quad \text{and} \quad g_{k-1,k-1} = \sqrt{(z_{k-1}, z_{k-1}) - \sum_{m=0}^{k-2} g_{m,k-1}^2}.$$

Given the set of vectors  $Z_{i-l+2}$ , the basis  $V_{i-l+1}$  can be extended to  $V_{i-l+2}$  by applying Theorem 1 with  $k = i-l+2$ . As soon as the dot products  $(z_{i-l+1}, v_j)$  for  $0 \leq j \leq i-2l+1$  and  $(z_{i-l+1}, z_j)$  for  $i-2l+1 < j \leq i-l+1$  are calculated, the vector  $v_{i-l+1}$  can be computed recursively as

$$(6) \quad v_{i-l+1} = \frac{z_{i-l+1} - \sum_{j=0}^{i-l} g_{j,i-l+1} v_j}{g_{i-l+1,i-l+1}},$$

i.e. using the identity  $Z_{i-l+2} = V_{i-l+2} G_{i-l+2}$ . For  $k > 0$ , the Hessenberg matrix  $H_{k+1,k}$  can be computed from the matrices  $H_{k,k-1}$ ,  $G_{k+1}$  and  $B_{k+1,k}$  in a column-wise fashion as follows.

**THEOREM 2.** [Ghysels et al. [24]] *Assume  $k > 0$ . Let  $G_{k+1}$  be the upper triangular basis transformation matrix for which  $Z_{k+1} = V_{k+1} G_{k+1}$  and let  $B_{k+1,k}$  be the upper Hessenberg matrix that connects the vectors in  $Z_k$  via  $A Z_k = Z_{k+1} B_{k+1,k}$ . Then the Hessenberg matrix for the basis  $V_{k+1}$  can be constructed column by column as*

$$(7) \quad H_{k+1,k} = \begin{bmatrix} H_{k,k-1} & (G_{k+1} b_{:,k-1} + g_{:,k} b_{k,k-1} - H_{k,k-1} g_{:,k-1}) g_{k-1,k-1}^{-1} \\ 0 & g_{k,k} b_{k,k-1} g_{k-1,k-1}^{-1} \end{bmatrix}.$$

*Proof.* This follows directly from  $H_{k+1,k} = G_{k+1} B_{k+1,k} G_k^{-1}$ , which is derived using the identity  $A V_k = V_{k+1} H_{k+1,k}$ , the transformation  $Z_{k+1} = V_{k+1} G_{k+1}$  and the relation  $A Z_k = Z_{k+1} B_{k+1,k}$ .

Once the Hessenberg matrix  $H_{i-l+2,i-l+1}$  has been computed, the basis  $Z_{i+1}$  can be extended to  $Z_{i+2}$  by adding the vector  $z_{i+1}$  that can be computed using the expression (3). The above considerations lead to the  $p(l)$ -GMRES algorithm shown in Alg. 1.

**REMARK 3. Krylov basis choice.** *The choice of appropriate shift values  $\sigma_i$  is vital to ensure numerical stability for the  $p(l)$ -GMRES algorithm. The monomial basis  $[v_0, A v_0, \dots, A^k v_0]$  for  $\mathcal{K}_{k+1}(v_0, A)$  may become ill-conditioned very quickly, which can be resolved by choosing an alternative basis of the form  $[v_0, P_1(A)v_0, \dots, P_k(A)v_0]$  such as the Newton basis  $P_i(A) = \prod_{j=0}^{i-1} (A - \sigma_j I)$ . Different shift choices  $\sigma_i$  are possible, e.g. the Ritz values of  $A$  or the zeros of the degree- $l$  Chebyshev polynomial. If all eigenvalues are located in  $[\lambda_{\min}, \lambda_{\max}]$  (excl. zero), the Chebyshev shifts are*

$$(8) \quad \sigma_i = \frac{\lambda_{\max} + \lambda_{\min}}{2} + \frac{\lambda_{\max} - \lambda_{\min}}{2} \cos\left(\frac{(2i+1)\pi}{2l}\right), \quad i = 0, \dots, l-1.$$

*More information can be found in the works by Hoemmen [34] and Ghysels et al. [24].*

**2.2. Deriving  $p(l)$ -CG from  $p(l)$ -GMRES.** We now derive the  $p(l)$ -CG algorithm starting from the Arnoldi procedure in  $p(l)$ -GMRES, Alg. 1, based on arguments that are similar to the ones used in the classical derivation of CG from GMRES, see e.g. [43, 48, 36].

**Algorithm 1** Pipelined GMRES method ( $p(l)$ -GMRES)

**Input:**  $A, b, x_0, l, m$ 


---

```

1:  $r_0 := b - Ax_0$ ;
2:  $v_0 := r_0 / \|r_0\|_2$ ;
3:  $z_0 := v_0$ ;  $g_{0,0} := 1$ ;
4: for  $i = 0, \dots, m + l$  do
5:    $z_{i+1} := \begin{cases} (A - \sigma_i I)z_i, & i < l \\ Az_i, & i \geq l \end{cases}$ 
6:   if  $i \geq l$  then
7:      $g_{j,i-l+1} := (g_{j,i-l+1} - \sum_{k=0}^{j-1} g_{k,j} g_{k,i-l+1}) / g_{j,j}; \quad j = i - 2l + 2, \dots, i - l$ 
8:      $g_{i-l+1,i-l+1} := \sqrt{g_{i-l+1,i-l+1} - \sum_{k=0}^{i-l} g_{k,i-l+1}^2}$ ;
9:     # Check for breakdown and restart if required
10:    if  $i < 2l$  then
11:       $h_{j,i-l} := (g_{j,i-l+1} + \sigma_{i-l} g_{j,i-l} - \sum_{k=0}^{i-l-1} h_{j,k} g_{k,i-l}) / g_{i-l,i-l}; \quad j = 0, \dots, i - l$ 
12:       $h_{i-l+1,i-l} := g_{i-l+1,i-l+1} / g_{i-l,i-l}$ ;
13:    else
14:       $h_{j,i-l} := (\sum_{k=0}^{i-2l+1} g_{j,k+l} h_{k,i-2l} - \sum_{k=j-1}^{i-l-1} h_{j,k} g_{k,i-l}) / g_{i-l,i-l}; \quad j = 0, \dots, i - l$ 
15:       $h_{i-l+1,i-l} := (g_{i-l+1,i-l+1} h_{i-2l+1,i-2l}) / g_{i-l,i-l}$ ;
16:    end if
17:     $v_{i-l+1} := (z_{i-l+1} - \sum_{j=0}^{i-l} g_{j,i-l+1} v_j) / g_{i-l+1,i-l+1}$ ;
18:     $z_{i+1} := (z_{i+1} - \sum_{j=0}^{i-l} h_{j,i-l} z_{j+l}) / h_{i-l+1,i-l}$ ;
19:    end if
20:     $g_{j,i+1} := \begin{cases} (z_{i+1}, v_j); & j = 0, \dots, i - l + 1 \\ (z_{i+1}, z_j); & j = i - l + 2, \dots, i + 1 \end{cases}$ 
21:  end for
22:  $y_m := \operatorname{argmin} \|H_{m+1,m} y_m - \|r_0\|_2 e_1\|_2$ ;
23:  $x_m := x_0 + V_m y_m$ ;

```

---

**2.2.1. Exploiting the symmetry: the Hessenberg matrix.** Application of  $p(l)$ -GMRES to a symmetric matrix  $A$  induces tridiagonalization of the Hessenberg matrix  $H_{i-l+2,i-l+1}$ . Thus only three Hessenberg elements need to be computed in each iteration  $i$  in lines 11/12 and 14/15 of Alg. 1, namely  $h_{i-l-1,i-l}$ ,  $h_{i-l,i-l}$  and  $h_{i-l+1,i-l}$ . Due to symmetry  $h_{i-l-1,i-l}$  equals  $h_{i-l,i-l-1}$ , which was already computed in iteration  $i-1$ . Furthermore, the ranges of the sums in the right-hand side of the expressions for  $h_{i-l,i-l}$  and  $h_{i-l+1,i-l}$ , see Alg. 1 line 11-15, are reduced significantly.

**COROLLARY 4.** *Let  $A$  be a symmetric matrix, let  $k > 0$  and let the matrices  $V_{k+1}$ ,  $Z_{k+1}$ ,  $G_{k+1}$ ,  $B_{k+1,k}$  and  $H_{k,k-1}$  as defined in Theorem 2 be available. Then the tridiagonal Hessenberg matrix  $H_{k+1,k}$  for the basis  $V_{k+1}$  can be constructed from  $H_{k,k-1}$  using the following expressions:*

$$(9) \quad h_{k-1,k-1} = \begin{cases} \sigma_{k-1} + (g_{k-1,k} - g_{k-2,k-1} h_{k-1,k-2}) / g_{k-1,k-1}, & k \leq l, \\ h_{k-l-1,k-l-1} + (g_{k-1,k} h_{k-l,k-l-1} - g_{k-2,k-1} h_{k-1,k-2}) / g_{k-1,k-1}, & k > l, \end{cases}$$

$$(10) \quad h_{k,k-1} = \begin{cases} g_{k,k} / g_{k-1,k-1}, & k \leq l, \\ (g_{k,k} h_{k-l,k-l-1}) / g_{k-1,k-1}, & k > l. \end{cases}$$

Note that for the cases  $k = 1$  and  $k = l + 1$  the values  $h_{0,-1}$  and  $h_{-1,0}$  should be considered zero.

*Proof.* It suffices to compute the entries  $h_{k-1,k-1}$  and  $h_{k,k-1}$  of  $H_{k+1,k}$ , since  $h_{k-2,k-1} = h_{k-1,k-2}$  due to symmetry and  $h_{j,k-1} = 0$  for  $0 \leq j \leq k-3$  since  $H_{k+1,k}$  is tridiagonal. The expressions (9) and (10) are derived directly from Theorem 2 using the fact that  $H_{k+1,k}$  is tridiagonal.  $\square$

Applying the above theorem with  $k = i - l + 1$  allows us to compute the Hessenberg matrix  $H_{i-l+2, i-l+1}$  in iteration  $i$ . The element  $h_{i-l, i-l}$  in  $H_{i-l+2, i-l+1}$  is characterized by expression (9):

$$(11) \quad h_{i-l, i-l} = \begin{cases} (g_{i-l, i-l+1} + \sigma_{i-l} g_{i-l, i-l} - g_{i-l-1, i-l} h_{i-l, i-l-1}) / g_{i-l, i-l}, & l \leq i < 2l, \\ (g_{i-l, i-l} h_{i-2l, i-2l} + g_{i-l, i-l+1} h_{i-2l+1, i-2l} - g_{i-l-1, i-l} h_{i-l, i-l-1}) / g_{i-l, i-l}, & i \geq 2l. \end{cases}$$

Note that for  $i = l$  the term  $-g_{i-l-1, i-l} h_{i-l, i-l-1} / g_{i-l, i-l}$  drops, while for  $i = 2l$  the term  $g_{i-l, i-l-1} h_{i-2l-1, i-2l} / g_{i-l, i-l}$  should be omitted. The update for  $h_{i-l+1, i-l}$  follows from (10) by setting  $k = i - l + 1$ , i.e.:

$$(12) \quad h_{i-l+1, i-l} = \begin{cases} g_{i-l+1, i-l+1} / g_{i-l, i-l}, & l \leq i < 2l, \\ (g_{i-l+1, i-l+1} h_{i-2l+1, i-2l}) / g_{i-l, i-l}, & i \geq 2l, \end{cases}$$

which is identical to the expressions on lines 12 and 15 in Alg. 1. In addition, the recurrence for the auxiliary basis vector  $z_{i+1}$ , given by (3) for the  $p(l)$ -GMRES method, can due to the symmetry of  $A$  be simplified to a three-term recurrence relation:

$$(13) \quad z_{i+1} = (Az_i - h_{i-l, i-l} z_i - h_{i-l-1, i-l} z_{i-1}) / h_{i-l+1, i-l}.$$

**2.2.2. The band structure of  $G_{i+1}$ .** The symmetry of the matrix  $A$  induces a particular band structure and symmetry for the upper triangular basis transformation matrix  $G_{i+1}$ .

LEMMA 5. *Let  $A$  be a symmetric matrix, assume  $i \geq l$  and let  $V_{i+1} = [v_0, v_1, \dots, v_i]$  be the orthogonal basis for  $\mathcal{K}_{i+1}(A, v_0)$ . Let  $Z_{i+1} = [z_0, z_1, \dots, z_i]$  be the auxiliary basis with  $z_i = P_l(A)v_{i-l}$  as defined by (2), then for all  $j \notin \{i-2l, i-2l+1, \dots, i-1, i\}$  it holds that  $g_{j,i} = (z_i, v_j) = 0$ .*

*Proof.* For symmetric  $A$  the matrix  $G_{i+1}$  is symmetric around its  $l$ -th upper diagonal, since

$$(14) \quad g_{j,i} = (z_i, v_j) = (P_l(A)v_{i-l}, v_j) = (v_{i-l}, P_l(A)v_j) = (v_{i-l}, z_{j+l}) = g_{i-l, j+l}.$$

As  $G_{i+1}$  is an upper triangular matrix, only the elements  $g_{i-2l, i}, g_{i-2l+1, i}, \dots, g_{i-1, i}, g_{i, i}$  differ from zero and  $G_{i+1}$  thus has a band structure with a band width of at most  $2l + 1$  non-zeros.  $\square$

For completeness we note that the alternative characterization of the matrix  $G_{i+1}$  (as a function of the matrix  $T_{i+1}$ ) derived in Appendix 6 may serve as an equivalent proof of Lemma 5.

The band structure of the matrix  $G_{i+1}$  further simplifies the algorithm. In the symmetric case the expression for  $g_{j, i-l+1}$  (see Alg. 1, line 7) that is derived from expression (5) reads:

$$(15) \quad g_{j, i-l+1} = \frac{g_{j, i-l+1} - \sum_{k=i-3l+1}^{j-1} g_{k, j} g_{k, i-l+1}}{g_{j, j}}, \quad j = i - 2l + 2, \dots, i - l,$$

where the sum includes only the non-zero elements  $g_{k, i-l+1}$  for which  $i - 3l + 1 \leq k \leq i - l + 1$ . The computation of  $g_{i-l+1, i-l+1}$  (Alg. 1, line 8), see (5), is treated in a similar way, yielding:

$$(16) \quad g_{i-l+1, i-l+1} = \sqrt{g_{i-l+1, i-l+1} - \sum_{k=i-3l+1}^{i-l} g_{k, i-l+1}^2}.$$

Furthermore, by exploiting the band structure of  $G_{i+1}$  for symmetric matrices  $A$ , the recurrence for  $v_{i-l+1}$  (Alg. 1, line 17), given in general by (6), is rewritten as:

$$(17) \quad v_{i-l+1} = \frac{z_{i-l+1} - \sum_{j=i-3l+1}^{i-l} g_{j, i-l+1} v_j}{g_{i-l+1, i-l+1}},$$

such that the recurrence for  $v_{i-l+1}$  is only based on the  $2l$  previous basis vectors  $v_{i-3l+1}, \dots, v_{i-l}$ .

Finally, since it follows from Lemma 5 that many entries of  $G_{i+1}$  effectively equal zero, only the dot products  $(z_{i+1}, z_j)$  and  $(z_{i+1}, v_j)$  (see Alg. 1, line 20) for which  $j = \max(0, i - 2l + 1), \dots, i + 1$  need to be computed in iteration  $i$  of the algorithm. We obtain

$$(18) \quad g_{j,i+1} = \begin{cases} (z_{i+1}, v_j), & j = \max(0, i - 2l + 1), \dots, i - l + 1, \quad (\text{only evaluated if } i \geq l - 1) \\ (z_{i+1}, z_j), & j = i - l + 2, \dots, i + 1. \end{cases}$$

**2.2.3. Towards p( $l$ )-CG.** To compute the solution  $x_m$  after the p( $l$ )-GMRES iteration has finished and the Krylov subspace basis  $V_m$  has been constructed, p( $l$ )-GMRES minimizes the Euclidean norm of the residual  $\|b - Ax_m\|_2$  over the Krylov subspace  $\mathcal{K}_m(A, r_0)$  as follows:

$$(19) \quad \min_{x_0 + V_m y_m \in \mathbb{R}^n} \|b - Ax_m\|_2 = \min_{y_m \in \mathbb{R}^m} \|r_0 - V_{m+1} H_{m+1,m} y_m\|_2 = \min_{y_m \in \mathbb{R}^m} \|\|r_0\|_2 e_1 - H_{m+1,m} y_m\|_2,$$

where  $y_m$  is a column vector of length  $m$ . This leads to a least squares minimization problem with an  $(m+1) \times m$  Hessenberg matrix, see Alg. 1, line 22. The construction of the solution  $x_m$  requires the *entire* Krylov subspace basis  $V_m$  in p( $l$ )-GMRES, which gives rise to a high storage overhead.

In contrast, in the Conjugate Gradient method the Ritz-Galerkin condition  $r_m = b - Ax_m \perp V_m$  together with the Lanczos relation  $AV_m = V_{m+1} T_{m+1,m}$  are used to find an expression for the approximate solution over the Krylov subspace  $x_0 + K_m(A, r_0)$ . More specifically, this implies:

$$(20) \quad 0 = V_m^T r_m = V_m^T (r_0 - AV_m y_m) = V_m^T (V_m (\|r_0\|_2 e_1 - T_m y_m)) = \|r_0\|_2 e_1 - T_m y_m,$$

resulting in  $y_m = T_m^{-1} \|r_0\|_2 e_1$  with a symmetric tridiagonal matrix  $T_m$ .

**REMARK 6. Relation to FOM and MINRES.** By modifying the p( $l$ )-GMRES algorithm by changing line 22 in Alg. 1 to  $y_m = H_{m,m}^{-1} \|r_0\|_2 e_1$  one immediately obtains a deep pipelined version of the so-called Full Orthogonalization Method (FOM), cf. [43]. In this section the p( $l$ )-CG method is derived as a symmetric variant of the FOM algorithm. As a side-note we also remark that by only exploiting the symmetry of the matrix but constructing the solution using the minimization procedure (19) like in Alg. 1 one could derive a pipelined version of the Minimal Residual method (MINRES) [41, 43], which can be applied to symmetric and indefinite systems. However, we focus on deriving a deep pipelined variant of the more widely used CG method in this work.

For notational convenience the elements of the matrix  $T_{i-l+2, i-l+1}$  are renamed in the symmetric setting. Denote  $\gamma_k := h_{k,k}$  and  $\delta_k := h_{k+1,k}$  for any  $0 \leq k \leq i-l$ . Then  $T_{i-l+2, i-l+1}$  is completely defined by the two arrays  $(\gamma_k)_{k=0, \dots, i-l}$  and  $(\delta_k)_{k=0, \dots, i-l}$ . The square symmetric tridiagonal matrix  $T_{i-l+1}$  is obtained by omitting the last row of the Hessenberg matrix  $T_{i-l+2, i-l+1}$ . Assume that the LU-factorization of the tridiagonal matrix  $T_{i-l+1} = L_{i-l+1} U_{i-l+1}$  is given by

$$(21) \quad \begin{pmatrix} \gamma_0 & \delta_0 & & & & \\ \delta_0 & \gamma_1 & \delta_1 & & & \\ & \delta_1 & \gamma_2 & \ddots & & \\ & & \ddots & \ddots & \delta_{i-l-1} & \\ & & & \delta_{i-l-1} & \gamma_{i-l} & \end{pmatrix} = \begin{pmatrix} 1 & & & & & \\ \lambda_1 & 1 & & & & \\ & \lambda_2 & 1 & & & \\ & & \ddots & \ddots & & \\ & & & \lambda_{i-l} & 1 & \end{pmatrix} \begin{pmatrix} \eta_0 & \delta_0 & & & & \\ & \eta_1 & \delta_1 & & & \\ & & \eta_2 & \ddots & & \\ & & & \ddots & \delta_{i-l-1} & \\ & & & & \eta_{i-l} & \end{pmatrix}.$$

Following the procedure outlined in [48, 36], and notably the derivation of D-Lanczos in [43], Sec. 6.7.1 (see also Remark 7), we now replace the minimization procedure (19) (Alg. 1, line 22) by

an iterative update of the solution  $x_{i-l+1}$  based on a search direction  $p_{i-l}$  as defined below. Note that  $\gamma_0 = \eta_0$  and it follows from (21) that  $\delta_{k-1} = \lambda_k \eta_{k-1}$  and that  $\gamma_k = \lambda_k \beta_k + \eta_k$ , or equivalently

$$(22) \quad \lambda_k = \delta_{k-1} / \eta_{k-1} \quad \text{and} \quad \eta_k = \gamma_k - \lambda_k \delta_{k-1}, \quad 1 \leq k \leq i-l.$$

These expressions allow to compute the elements of the lower/upper triangular matrices  $L_{i-l+1}$  and  $U_{i-l+1}$ . From (20) it follows that the approximate solution  $x_{i-l+1}$  is given by

$$(23) \quad x_{i-l+1} = x_0 + V_{i-l+1} y_{i-l+1} = x_0 + V_{i-l+1} U_{i-l+1}^{-1} L_{i-l+1}^{-1} \|r_0\|_2 e_1 = x_0 + P_{i-l+1} q_{i-l+1},$$

where the search directions are defined as  $P_{i-l+1} := V_{i-l+1} U_{i-l+1}^{-1}$  and  $q_{i-l+1} := L_{i-l+1}^{-1} \|r_0\|_2 e_1$ . Note that  $p_0 = v_0 / \eta_0$ . The columns  $p_k$  (for  $1 \leq k \leq i-l$ ) of  $P_{i-l+1}$  can easily be computed recursively. Indeed, since  $P_{i-l+1} U_{i-l+1} = V_{i-l+1}$ , it follows that  $v_k = \delta_{k-1} p_{k-1} + \eta_k p_k$  for any  $1 \leq k \leq i-l$ , yielding the recurrence for the search directions  $p_k$ :

$$(24) \quad p_k = \eta_k^{-1} (v_k - \delta_{k-1} p_{k-1}), \quad 1 \leq k \leq i-l.$$

Denoting the elements of the vector  $q_{i-l+1}$  by  $[\zeta_0, \dots, \zeta_{i-l}]^T$ , it follows from  $L_{i-l+1} q_{i-l+1} = \|r_0\|_2 e_1$  that  $\zeta_0 = \|r_0\|_2$  and  $\lambda_k \zeta_{k-1} + \zeta_k = 0$  for  $1 \leq k \leq i-l$ . Hence, the scalar  $\zeta_k$  is computed in each iteration using the recursion:

$$(25) \quad \zeta_k = -\lambda_k \zeta_{k-1}, \quad 1 \leq k \leq i-l.$$

Using the search direction  $p_{i-l}$  and the scalar  $\zeta_{i-l}$ , which are both updated recursively in each iteration, the approximate solution  $x_{i-l+1}$  is updated using the recurrence relation:

$$(26) \quad x_{i-l+1} = x_{i-l} + \zeta_{i-l} p_{i-l}.$$

By merging this recursive update for the solution with the simplifications suggested in Sections 2.2.1 and 2.2.2, we obtain a new iterative scheme which we will denote as  $l$ -length pipelined CG, or  $p(l)$ -CG for short. The corresponding algorithm is shown in Alg. 2.

**REMARK 7. CG vs. D-Lanczos.** *An important remark on nomenclature should be made here. As indicated earlier, Alg. 2 is mathematically equivalent (i.e. in exact arithmetic) to the direct Lanczos (or D-Lanczos) method [43], rather than the CG method. Indeed, Alg. 2 could alternatively be called ‘p(l)-D-Lanczos’. The difference between the two methods is subtle. Unlike classic CG the D-Lanczos algorithm may break down even in exact arithmetic due to a possible division by zero in the recurrence relation (24), which stems from implicit Gaussian elimination without pivoting. Apart from this possible (yet rarely occurring) instability, Alg. 2 is mathematically equivalent to CG and their convergence histories coincide (for any choice of  $l$ ), see Fig. 1. Since Alg. 2 is intrinsically based on residual orthogonality and search direction  $A$ -orthogonality (i.e. the key properties of the CG method), we denote Alg. 2 as  $p(l)$ -CG. Alternative formulations of the CG algorithm could be used to derive other pipelined variants that are mathematically equivalent to CG. For example, three-term Conjugate Gradients [43] can be rewritten into a pipelined variant that produces iterates identical to those of CG in exact arithmetic; we do not expound on the details of this method here.*

**REMARK 8. Square root breakdown.** *Unlike other more common variants of the CG algorithm [42, 38, 8, 25], the  $p(l)$ -CG method computes a square root to calculate  $g_{i-l+1, i-l+1}$  (Alg. 2, line 8) and may break down when the root argument becomes negative or zero, just like  $p(l)$ -GMRES.*

**Algorithm 2** Pipelined Conjugate Gradient method (p(l)-CG)**Input:**  $A, b, x_0, l, m$ 


---

```

1:  $r_0 := b - Ax_0$ ;
2:  $v_0 := r_0 / \|r_0\|_2$ ;
3:  $z_0 := v_0$ ;  $g_{0,0} := 1$ ;
4: for  $i = 0, \dots, m + l$  do
5:    $z_{i+1} := \begin{cases} (A - \sigma_i I)z_i, & i < l \\ Az_i, & i \geq l \end{cases}$ 
6:   if  $i \geq l$  then
7:      $g_{j,i-l+1} := (g_{j,i-l+1} - \sum_{k=i-3l+1}^{j-1} g_{k,j} g_{k,i-l+1}) / g_{j,j}; \quad j = i - 2l + 2, \dots, i - l$ 
8:      $g_{i-l+1,i-l+1} := \sqrt{g_{i-l+1,i-l+1} - \sum_{k=i-3l+1}^{i-l} g_{k,i-l+1}^2}$ ;
9:     # Check for breakdown and restart if required
10:    if  $i < 2l$  then
11:       $\gamma_{i-l} := (g_{i-l,i-l+1} + \sigma_{i-l} g_{i-l,i-l} - g_{i-l-1,i-l} \delta_{i-l-1}) / g_{i-l,i-l}$ ;
12:       $\delta_{i-l} := g_{i-l+1,i-l+1} / g_{i-l,i-l}$ ;
13:    else
14:       $\gamma_{i-l} := (g_{i-l,i-l} \gamma_{i-2l} + g_{i-l,i-l+1} \delta_{i-2l} - g_{i-l-1,i-l} \delta_{i-l-1}) / g_{i-l,i-l}$ ;
15:       $\delta_{i-l} := (g_{i-l+1,i-l+1} \delta_{i-2l}) / g_{i-l,i-l}$ ;
16:    end if
17:     $v_{i-l+1} := (z_{i-l+1} - \sum_{j=i-3l+1}^{i-l} g_{j,i-l+1} v_j) / g_{i-l+1,i-l+1}$ ;
18:     $z_{i+1} := (z_{i+1} - \gamma_{i-l} z_i - \delta_{i-l-1} z_{i-1}) / \delta_{i-l}$ ;
19:  end if
20:   $g_{j,i+1} := \begin{cases} (z_{i+1}, v_j); & j = \max(0, i - 2l + 1), \dots, i - l + 1 \\ (z_{i+1}, z_j); & j = i - l + 2, \dots, i + 1 \end{cases}$ 
21:  end if
22:  if  $i = l$  then
23:     $\eta_0 := \gamma_0$ ;
24:     $\zeta_0 := \|r_0\|_2$ ;
25:     $p_0 := v_0 / \eta_0$ ;
26:  else if  $i \geq l + 1$  then
27:     $\lambda_{i-l} := \delta_{i-l-1} / \eta_{i-l-1}$ ;
28:     $\eta_{i-l} := \gamma_{i-l} - \lambda_{i-l} \delta_{i-l-1}$ ;
29:     $\zeta_{i-l} := -\lambda_{i-l} \zeta_{i-l-1}$ ;
30:     $p_{i-l} := (v_{i-l} - \delta_{i-l-1} p_{i-l-1}) / \eta_{i-l}$ ;
31:     $x_{i-l} := x_{i-l-1} + \zeta_{i-l-1} p_{i-l-1}$ ;
32:  end if
33: end for

```

---

When  $g_{i-l+1,i-l+1} - \sum_{k=i-3l+1}^{i-l} g_{k,i-l+1}^2 = 0$  (or sufficiently close to zero in finite precision arithmetic) a happy breakdown occurs, implying the solution has been found. A value smaller than zero signals loss of basis orthogonality and results in a hard breakdown caused by numerical rounding errors in finite precision arithmetic. In this case the algorithm has not converged and a restart or a re-orthogonalization of the Krylov subspace basis is required. In this work we opt for an explicit restart when a square root breakdown occurs, using the last computed solution  $x_k$  as the new initial guess. Other restart or re-orthogonalization strategies are possible [2, 43], but are beyond the scope of this work. We stress that the square root breakdown is intrinsic to the pipelining procedure and that it is unrelated to the possible instability in the D-Lanczos method pointed out in Remark 7.

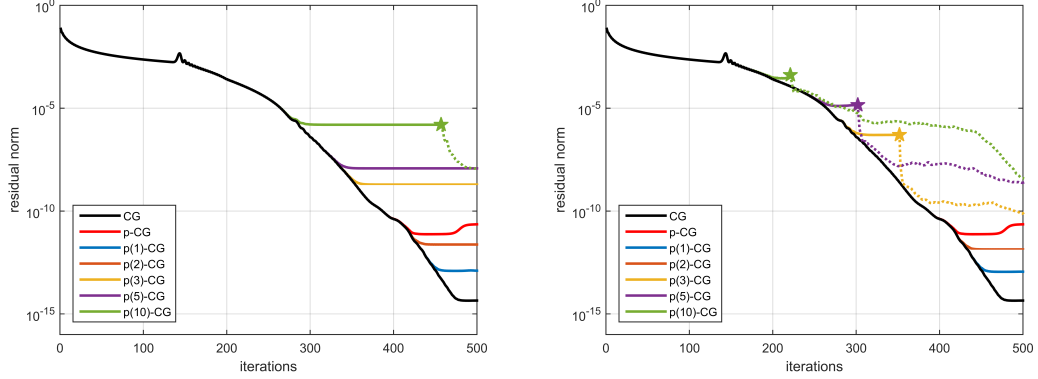


FIG. 1. Comparison of the residual norm history  $\|b - Ax_j\|$  for different CG variants for a 2D Poisson problem with  $200 \times 200$  unknowns. The stabilizing shifts  $\sigma_i$  for  $p(\ell)$ -CG are based on the degree  $l$  Chebyshev polynomial on the interval  $[0, 8]$  (left) (optimal shift choices) and the perturbed interval  $[0, 8 * 1.005]$  (right) (slightly sub-optimal shifts). Square root breakdowns in  $p(\ell)$ -CG are indicated by a  $\star$  symbol (followed by explicit iteration restart).

**2.2.4. The residual norm in  $p(l)$ -CG.** The derivation of the  $p(l)$ -CG method follows the classic procedure from [43, 48, 36] but does not include a recurrence relation for the residual, similarly to the  $p(l)$ -GMRES algorithm. This is in contrast with most (communication reducing) variants of CG, where the residual is typically computed recursively in each iteration to update the solution, see e.g. [25, 7] and Remark 10. However, the residual norm is a useful measure of deviation from the solution that allows (among others) to formulate stopping criteria. Adding an extra SPMV to explicitly compute the residual in each iteration is not advisable, since it would increase the algorithm's computational cost. The following property allows to compute the residual norm in each iteration of the  $p(l)$ -CG algorithm without the explicit computation of the residual vector.

**THEOREM 9.** Let the search directions  $P_{i-l+1}$  of the  $p(l)$ -CG method be defined by  $p_0 = v_0/\eta_0$  and the recurrence (24), i.e.  $p_k = \eta_k^{-1}(v_k - \beta_k p_{k-1})$ , for  $1 \leq k \leq i-l$ . Let the solution  $x_{i-l+1}$  be given by  $x_{i-l+1} = x_0 + P_{i-l+1} q_{i-l+1}$ , where  $q_{i-l+1} = (\zeta_0, \dots, \zeta_{i-l})^T$  is characterized by the entries  $\zeta_0 = \|r_0\|_2$  and  $\zeta_k = -\lambda_k \zeta_{k-1}$ . Then it holds that  $|\zeta_k| = \|r_k\|_2$  in any iteration  $0 \leq k \leq i-l$ .

*Proof.* The first part of the proof follows the classic argumentation of Saad in [43], p.160. The residual  $r_k$  with  $0 \leq k \leq i-l$  is given by:

$$\begin{aligned} r_k &= b - Ax_k = b - A(x_0 + V_k y_k) = r_0 - AV_k y_k \\ &= \|r_0\|_2 v_0 - V_k T_k y_k - \delta_{k-1} (e_k^T y_k) v_k = -\delta_{k-1} (e_k^T y_k) v_k, \quad 0 \leq k \leq i-l, \end{aligned}$$

where the last equality holds since  $\|r_0\|_2 v_0 - V_k T_k y_k = 0$ , see (20). Since  $v_k$  is normalized, i.e.  $\|v_k\|_2 = 1$ , it holds that  $\|r_k\|_2 = |-\delta_{k-1} (e_k^T y_k)|$ . From the definition  $y_k = U_k^{-1} q_k$  it follows that the last element of  $y_k$  is  $\zeta_{k-1}/\eta_{k-1}$ . Hence  $\|r_k\|_2 = |-\zeta_{k-1} \delta_{k-1}/\eta_{k-1}| = |-\zeta_{k-1} \lambda_k| = |\zeta_k|$ .  $\square$

The equality  $|\zeta_k| = \|r_k\|_2$  holds in exact arithmetic, but rounding errors may contaminate  $\zeta_k$  in a practical implementation in each iteration, leading to deviations from the actual residual norm. We expound on the numerical behavior of the  $p(l)$ -CG method in finite precision in Section 4.

**REMARK 10. Comparison to  $p$ -CG from Ghysels et al. [25].** Introducing a recurrence relation for the residual and rewriting the corresponding expression to achieve an overlap between

global communication and SPMV computation would lead to the pipelining approach proposed in [25] to derive the  $p$ -CG and  $p$ -CR methods (which are limited to a pipeline length  $l = 1$ ). Although the  $p$ -CG and  $p(l)$ -CG variants are both denoted as ‘pipelined CG methods’, the approach to pipelining proposed in this work fundamentally differs from the procedure in [25] and the resulting algorithms are quite different from a numerical perspective.

**REMARK 11. Stopping criterion.** The characterization of the residual norm  $\|r_{i-l}\|_2 = |\zeta_{i-l}|$  allows to add a stopping criterion to Alg. 2. Given a relative residual tolerance  $\tau$  (input variable), the following classic stopping criterion can for example be added after line 31 in Alg. 2:

**if**  $|\zeta_{i-l}|/\|b\|_2 \leq \tau$  **then** BREAK **end if**.

Note that the location of the stopping criterion in the algorithm is important. Indeed, the above check could be performed immediately after  $\zeta_{i-l}$  has been computed in Alg. 2 on line 29; however, the update of the solution  $x_{i-l}$  that corresponds to the residual  $|\zeta_{i-l}|$  is only computed on line 31.

**REMARK 12. Solution update.** In light of Remark 11 and the discussion in Section 2.2.3, note that one could already compute the next solution  $x_{i-l+1} = x_{i-l} + \zeta_{i-l}p_{i-l}$ , see (23)-(26), on line 31 of Alg. 2, since  $p_{i-l}$  and  $\zeta_{i-l}$  are both computed in iteration  $i$ . However, the corresponding residual norm  $|\zeta_{i-l+1}|$  is then available only after executing line 29 in iteration  $i + 1$  (where the stopping criterion could be checked). To keep the solution and residual norm within a single iteration in sync and retain the analogy with Alg. 1 we opt to compute the solution  $x_{i-l}$  in iteration  $i$  in Alg. 2.

**2.3. Preconditioned  $p(l)$ -CG.** Since preconditioning is a crucial aspect for the efficient solution of large scale linear systems, we discuss the extension of the  $p(l)$ -CG algorithm to include a preconditioner. The methodology follows the derivation of the preconditioned CG and  $p$ -CG methods outlined in e.g. [25], aiming to iteratively solve the system  $M^{-1}Ax = M^{-1}b$  where both  $A$  and  $M$  are symmetric positive definite matrices. The approximate solutions  $x_i$  ( $i \geq 0$ ) lie in the subspaces  $x_0 + \mathcal{K}_i(M^{-1}A, r_0)$ . However, the symmetry of  $A$  and  $M$  in general does not imply that the preconditioned system is symmetric. To preserve symmetry we use the observation that  $M^{-1}A$  is self-adjoint with respect to the  $M$  inner product  $(x, y)_M = (Mx, y) = (x, My)$ .

Let  $V_{i-l+1} = [v_0, \dots, v_{i-l}]$  again be the orthonormal basis for the  $(i-l+1)$ -th Krylov subspace  $\mathcal{K}_{i-l+1}(M^{-1}A, r_0)$ . Note that  $r_i$  denotes the preconditioned residual  $M^{-1}(b - Ax_i)$  in this section. We define the auxiliary basis  $Z_{i+1} = [z_0, z_1, \dots, z_i]$  similarly to (2):

$$(27) \quad z_j := \begin{cases} v_0, & j = 0, \\ P_j(M^{-1}A)v_0, & 0 < j \leq l, \\ P_l(M^{-1}A)v_{j-l}, & j > l, \end{cases} \quad \text{with} \quad P_i(t) := \prod_{j=0}^{i-1} (t - \sigma_j), \quad \text{for } i \leq l,$$

The recurrence relations (3) and (13) can in the preconditioned case be summarized as:

$$(28) \quad z_{i+1} = \begin{cases} (M^{-1}A - \sigma_i I)z_i & i < l \\ (M^{-1}Az_i - \gamma_{i-l}z_i - \delta_{i-l-1}z_{i-1})/\delta_{i-l} & i \geq l. \end{cases}$$

In addition to the basis  $Z_{i+1}$ , the *unpreconditioned* auxiliary basis vectors  $\hat{Z}_{i+1} = [\hat{z}_0, \hat{z}_1, \dots, \hat{z}_i]$  are defined as  $\hat{z}_j = Mz_j$  such that

$$(29) \quad z_j = M^{-1}\hat{z}_j, \quad j \leq i.$$

The matrix  $M$  (preconditioner inverse) is generally not explicitly available; however, for  $i = 0$  the first auxiliary vectors  $\hat{z}_0$  and  $z_0$  can be computed as  $\hat{z}_0 = Mr_0/\|r_0\|_M = (b - Ax_0)/\|r_0\|_M$  and

$z_0 = M^{-1}\hat{z}_0$ . By multiplying both sides in the recurrence relations (28) for  $z_{i+1}$  by  $M$  one readily derives recurrence relations for the unpreconditioned basis vector  $\hat{z}_{i+1}$ :

$$(30) \quad \hat{z}_{i+1} = \begin{cases} Az_i - \sigma_i \hat{z}_i & i < l \\ (Az_i - \gamma_a \hat{z}_i - \delta_{a-1} \hat{z}_{i-1})/\delta_a & i \geq l. \end{cases}$$

The preconditioned auxiliary basis vector  $z_{i+1}$  can be computed after the SPMV  $Az_i$  has been computed by applying the preconditioner to  $Az_i$  and using expression (28). Given the basis vectors  $V_{i-l+1}$ ,  $\hat{Z}_{i+1}$  and  $Z_{i+1}$ , we replace the usual Euclidean dot product in Alg. 2 with the  $M$  dot product. The dot products  $g_{j,i+1}$  for  $0 \leq j \leq i+1$  are then computed in analogy to (18) as follows:

$$(31) \quad g_{j,i+1} = \begin{cases} (z_{i+1}, v_j)_M = (\hat{z}_{i+1}, v_j), & j = \max(0, i-2l+1), \dots, i-l+1, \\ (z_{i+1}, z_j)_M = (\hat{z}_{i+1}, v_j), & j = i-l+2, \dots, i+1. \end{cases}$$

With the above definitions, Lemma 5 holds for the preconditioned pipelined CG method with the adapted definition  $g_{j,i} = (z_i, v_j)_M = (\hat{z}_i, v_j)$ . Consequently, the preconditioned  $p(l)$ -CG algorithm is a direct extension of Alg. 2, with reformulated dot products and the addition of the recurrence relation (30) for the unpreconditioned auxiliary variable  $\hat{z}_{i+1}$ .

Note that Theorem 9 still holds for the preconditioned system when the Euclidean 2-norm of  $r_k$  in the formulation of the theorem is replaced by the  $M$ -norm of  $r_k$ . That is: for any iteration  $k$  in preconditioned  $p(l)$ -CG it holds that  $|\zeta_k| = \|r_k\|_M = \sqrt{(b - Ax_k, M^{-1}(b - Ax_k))}$ . The preconditioned algorithm thus intrinsically computes the  $M$ -norm of the residual in each iteration.

**REMARK 13. *Newton basis shifts.*** *The preconditioned linear system also allows for the use of a shifted Newton-type basis for the polynomials  $P_i(M^{-1}A)$  that are used to define  $\hat{z}_{i+1}$  and  $z_{i+1}$  as illustrated by (28) and (30). However, since the preconditioner application also overlaps with global communication, it may not be required to use deep pipelines in practice when the preconditioner application is sufficiently computationally expensive with respect to the global reduction phase.*

**3. Implementation considerations.** Section 2 gave an overview of the mathematical properties of the  $p(l)$ -CG method, ultimately leading to Alg. 2. In this section we comment on several important technical aspects concerning the implementation of the  $p(l)$ -CG algorithm.

**3.1. Hiding communication in  $p(l)$ -CG.** Alg. 2 gives the classic algebraic formulation of the  $p(l)$ -CG method. However, it may not be directly apparent from this formulation where the overlap of global communication with computational work occurs throughout the algorithm. We therefore introduce a schematic kernel-based representation of the  $p(l)$ -CG algorithm in this section. The following computational kernels are defined in iteration  $i$  in Alg. 2:

kernel #	kernel type	kernel description	Alg. 2 lines
(K1)	SPMV	apply $A$ and $M^{-1}$ to compute $z_{i+1}$ and $\hat{z}_{i+1}$	5
(K2)	SCALAR	update basis transformation matrix $G_{i-l+2}$ elements	7-8
(K3)	SCALAR	update Hessenberg matrix $H_{i-l+2, i-l+1}$ elements	10-16
(K4)	AXPY	recursive update of $v_{i-l+1}$ , $z_{i+1}$ and $\hat{z}_{i+1}$	17-18
(K5)	DOTPR	compute dot products $(\hat{z}_{i+1}, z_j)$ and $(\hat{z}_{i+1}, v_j)$	20
(K6)	AXPY	update solution $x_{i-l}$ and residual norm $ \zeta_{i-l} $	22-32

The SPMV kernel (K1) is considered to be the most computationally intensive part of the algorithm, and hence should be overlapped with the global reduction phase in (K5) to hide communication

---

**Algorithm 3** Schematic representation of  $p(l)$ -CG **Input:**  $A, M^{-1}, b, x_0, l, m$

---

```

1: INITIALIZATION ;
2: for  $i = 0, \dots, m + l$  do
3:   (K1) SPMV ;
4:   if  $i \geq l$  then
5:     MPI.Wait(req(i-l), ...) ;
6:     (K2) SCALAR ;
7:     (K3) SCALAR ;
8:     (K4) AXPY ;
9:   end if
10:  (K5) DOTPR ;
11:  MPI_Iallreduce(..., G(max(0,i-2l+1):i+1,i+1), ..., req(i)) ;
12:  (K6) AXPY ;
13: end for

```

---

latency and idle core time. Kernels (K2), (K3), (K4) and (K6) represent purely local scalar and vector operations which are assumed to be executed very fast on multi-node hardware. These operations are also overlapped with the global reduction phase; however, due to their low arithmetic complexity the overlap is not expected to yield any major performance improvement. In (K5) all local contributions to the dot products are first computed by each worker. Subsequently a global reduction phase is performed in which local contributions are added pairwise via a  $\log_2(N)$  length reduction tree, where  $N$  represents the number of workers. Once the scalar result of each dot product has been collected on a single worker, a global broadcasting phase redistributes the resulting scalars back to all workers for local use in the next iteration. The preconditioned  $p(l)$ -CG algorithm can be summarized schematically using these kernel definitions as displayed in Alg. 3.

Our implementation uses MPI with the MPI-3 standard as the communication library. The MPICH-3 library used in our experiments, see Section 5, allows for asynchronous progress in the global reduction by setting the following environment variables:

```

MPICH_ASYNC_PROGRESS=1;
MPICH_MAX_THREAD_SAFETY=multiple;

```

Global communication is initiated by a call which starts a non-blocking reduction:

```

MPI_Iallreduce(..., G(i-2l+1:i+1,i+1), ..., req(i));

```

The input argument  $G(i-2l+1:i+1,i+1)$  represents the  $2l + 1$  elements of the band structured matrix  $G_{i+2}$  that are computed using the dot products in (K5) in iteration  $i$ , see (31). The result of the corresponding global reduction phase is signaled to be due to arrive by the call to

```

MPI.Wait(req(i), ...);

```

The `MPI_Request` array element `req(i)` that is passed as an input argument to `MPI.Wait` keeps track of the iteration index in which the global reduction phase was initiated. Since the  $p(l)$ -CG method overlaps  $l$  SPMV's with a single global reduction phase, the call to `MPI.Wait(req(i), ...)` occurs effectively in iteration  $i + l$ , i.e.  $l$  iterations after the call `MPI_Iallreduce(..., req(i))`.

The schematic representation, Alg. 3, shows that the global reduction phase that is initiated by `MPI_Iallreduce` with request `req(i)` in iteration  $i$  overlaps with a total of  $l$  SPMV's, namely the kernels (K1) in iterations  $i + 1$  up to  $i + l$ . The corresponding call to `MPI.Wait` with request

	GLRED	SPMV	TIME (GLRED & SPMV)	FLOPS (AXPY & DOTPR)	MEMORY
CG	2	1	2 GLRED + 1 SPMV	10	3
p-CG	1	1	max(GLRED, SPMV)	16	6
p( $l$ )-CG	1	1	max(GLRED/ $l$ , SPMV)	$6l + 10$	$3l + 3$
p( $l$ )-GMRES	1	1	max(GLRED/ $l$ , SPMV)	$6i - 4l + 8$	$2i - l + 4$

TABLE 1

Theoretical specifications comparing p( $l$ )-CG to related Krylov subspace methods. ‘CG’ denotes classic CG; ‘p-CG’ is the pipelined CG method from [25]; ‘p( $l$ )-CG’ (with  $l \geq 1$ ) denotes Alg. 2; ‘p( $l$ )-GMRES’ is Alg. 1. GLRED: number of global all-reduce communication phases per iteration; SPMV: number of SPMVs per iteration; TIME: time spent per iteration in GLREDS and SPMVs; FLOPS: number of flops ( $\times n$ ) per iteration for AXPYS and dot products ( $i$  = iteration index); MEMORY: total number of vectors in memory (excl.  $x_i$  and  $b$ ) during execution.

$\text{req}((i+1)-1) = \text{req}(i)$  takes place in iteration  $i+l$  before the computations of (K2) in which the dot product results are required, but after the SPMV kernel (K1) has been executed. In each iteration the global reduction also overlaps with a number of less computationally intensive operations from (K2), (K3), (K4) and (K6). Hence, the global communication latency of the dot products in (K5) is ‘hidden’ behind the computational work of  $l$  p( $l$ )-CG iterations.

Table 1 summarizes key theoretical properties of the p( $l$ )-CG method in comparison to related algorithms (incl. memory requirements – see Section 3.2). The FLOPS count reported for p( $l$ )-CG assumes that the symmetry of  $G_{i+1}$ , see Lemma 5, is exploited to reduce the number of dot products that are computed in Alg. 2, line 20. The  $l$  elements  $g_{i-2l+1,i+1}, \dots, g_{i-l,i+1}$  have already been computed in previous iterations, see expression (14). Note that the results for the p( $l$ )-GMRES algorithm exclude the computational and storage cost to execute line 22-23 in Alg. 1.

**3.2. Storing the  $V_k$  and  $Z_k$  basis.** A clear advantage of the pipelined p( $l$ )-CG method, Alg. 2, in comparison with p( $l$ )-GMRES, Alg. 1, is its reduced storage requirements. In p( $l$ )-GMRES the complete bases  $V_{i-l+1}$  and  $Z_{i+1}$  need to be built and stored during the entire run of the algorithm, since all basis vectors are needed in the recursions for the next basis vectors (see Alg. 1 lines 17, 18 and 20). In contrast, the symmetry of the matrix  $A$  induces the symmetry of the matrix  $T_k$ , see Corollary 4, which in turn induces a band structure for  $G_k$  as shown in Theorem 5. In the  $i$ -th iteration of Alg. 2 the new vector  $z_{i+1}$  is computed by an SPMV with  $z_i$  (line 5); subsequently  $z_{i-l+1}$  and  $v_{i-3l+1}, v_{i-3l+2}, \dots, v_{i-l}$  are required to compute the next basis vector  $v_{i-l+1}$ , which itself also needs to be stored (line 17); next the last three auxiliary vectors  $z_{i-1}, z_i$  and  $z_{i+1}$  are used in the recurrence for  $z_{i+1}$  (line 18); and finally the vectors  $v_{i-l+1}$  and  $z_{i-l+2}, \dots, z_{i+1}$  are needed to compute the dot products (line 20). This implies that the  $3l+2$  basis vectors  $\{v_{i-3l+1}, \dots, v_{i-l+1}\} \in V_{i-l+2}$  and  $\{z_{i-l+1}, \dots, z_{i+1}\} \in Z_{i+2}$  are required in iteration  $i$ . From iteration  $i$  onward basis vectors  $v_j$  with indices  $j < i-3l+1$ , and vectors  $z_j$  with  $j < i-l+1$  are not used in either the recursive vector updates or the dot products in Alg. 2, and should thus no longer be stored. Hence, no more than  $3l+2$  basis vectors need to be kept in memory in *any* iteration of the p( $l$ )-CG algorithm. Fig. 2 schematically shows the storage requirements in iteration  $i$  of Alg. 2. In each iteration an auxiliary vector  $z_{i+1}$  is added and a new sequence of dot products is initiated. The results of the dot product calculations arrive  $l$  iterations later, see Section 3.1. Dot products that were initiated  $l$  iterations ago are then used to append a basis vector  $v_{i-l+1}$ .

REMARK 14. **Storage in preconditioned p( $l$ )-CG.** A similar analysis of basis storage requirements can be performed for the preconditioned version of p( $l$ )-CG. In addition to the  $3l+2$  vectors from the bases  $V_{i-j+2}$  and  $Z_{i+2}$  pointed out above, only the last three vectors  $\hat{z}_{i-1}, \hat{z}_i$  and

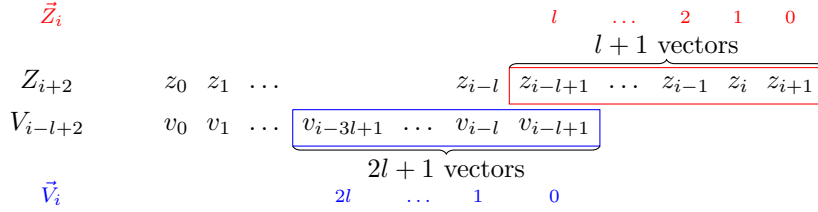


FIG. 2. The sequence of auxiliary vectors  $Z_{i+2}$  and basis vectors  $V_{i-l+2}$  constructed in the  $i$ -th iteration of  $p(l)$ -CG, Alg. 2. Colored boxes represent vectors that are actively used in iteration  $i$  and thus should be kept in memory up to this point, see Section 3.2. They are collected in the sliding windows  $\vec{Z}_i$  and  $\vec{V}_i$ , see Appendix 6. The super- and sub-indices indicate the position of the corresponding vectors in the sliding windows.

$\hat{z}_{i+1}$  in the auxiliary basis  $\hat{Z}_i$  are required in the recursive update for  $\hat{z}_{i+1}$ . Vectors  $\hat{z}_j$  with  $j < i - 1$  are not used in current or future iterations of the algorithm from iteration  $i$  onward. Hence, the preconditioned algorithm stores a maximum of  $3l + 5$  basis vectors at any point during the algorithm, and thus a total of  $3l + 6$  vectors are kept in MEMORY, cf. Table 1.

In Appendix 6 we comment on an efficient way to implement the storage of the basis vectors throughout the algorithm by using the concept of ‘sliding windows’.

**4. Analysis of the attainable accuracy of  $p(l)$ -CG in finite precision arithmetic.** As suggested by Fig. 1, replacing the classic CG algorithm by the pipelined  $p(l)$ -CG variant introduces numerical issues. The numerical accuracy attainable by the  $p(l)$ -CG method may be reduced drastically for larger pipeline lengths  $l$ . In exact arithmetic (and provided no square root breakdowns occur in  $p(l)$ -CG, see Remark 8),  $p(l)$ -CG produces a series of iterates identical to the classic CG method. However, in finite precision arithmetic their behavior can differ significantly as local rounding errors may induce a decrease in attainable accuracy and a delay of convergence. The impact of finite precision round-off errors on the numerical stability of classic CG has been extensively studied [26, 29, 27, 32, 46, 47, 40, 23]. In communication reducing CG variants the effects of local rounding errors are significantly amplified; we refer to our manuscript [12] and the work by Carson et al. [6] for an overview of the stability analysis of the depth one pipelined Conjugate Gradient method from [25]. In this section we analyze the behavior of local rounding errors that stem from the multi-term recurrence relations in the  $p(l)$ -CG algorithm in a finite precision framework. Preconditioning is omitted in this section for simplicity of notation but without loss of generality.<sup>1</sup>

In this section we use a notation with bars to indicate variables that are computed in a finite precision setting. Furthermore, for variables that are defined recursively in the algorithm, we differentiate between the recursively computed variable and the ‘actual’ variable, i.e. the variable that would be produced by exact computation using already computed inaccurate quantities. The latter is denoted by a bold typesetting. E.g. the recursively computed residual in finite precision is denoted as  $\bar{r}_j$ , whereas the actual residual (which *could* be computed, but typically isn’t to reduce computational cost) is  $\bar{\mathbf{r}}_j = b - A\bar{x}_j$ . The primary aim of this section is to analyze the gap between the recursively computed variable  $\bar{r}_j$  and its local ‘recurrence error-free’ counterpart  $\bar{\mathbf{r}}_j$ .

We use the classic model for floating point arithmetic with machine precision  $\epsilon$ . The round-off error on scalar multiplication, vector summation, SPMV application and dot product computation

<sup>1</sup>The extension of the local rounding error analysis to the preconditioned  $p(l)$ -CG algorithm is trivial since the recurrences for the unpreconditioned variables are decoupled from their preconditioned counterparts. We refer the reader to Section 2.3 and our related work in [12] for more details.

on an  $n$ -by- $n$  matrix  $A$ , length  $n$  vectors  $v$ ,  $w$  and a scalar number  $\alpha$  are respectively bounded by

$$\begin{aligned} \|\alpha v - \text{fl}(\alpha v)\| &\leq \|\alpha v\| \epsilon = |\alpha| \|v\| \epsilon, & \|v + w - \text{fl}(v + w)\| &\leq (\|v\| + \|w\|) \epsilon, \\ \|Av - \text{fl}(Av)\| &\leq \mu\sqrt{n} \|A\| \|v\| \epsilon, & |(v, w) - \text{fl}((v, w))| &\leq n \|v\| \|w\| \epsilon, \end{aligned}$$

where  $\text{fl}(\cdot)$  indicates the finite precision floating point representation,  $\mu$  is the maximum number of nonzeros in any row of  $A$ , and the norm  $\|\cdot\|$  represents the Euclidean 2-norm in this section.

**4.1. Local rounding error behavior in finite precision p( $l$ )-CG.** We give a very summarily overview of the behavior of local rounding errors in classic CG, see e.g. [29, 46, 47, 40]. The recurrence relations for the approximate solution  $\bar{x}_{j+1}$  and the residual  $\bar{r}_{j+1}$  computed by the *classic* CG algorithm in the finite precision framework are

$$(32) \quad \bar{x}_{j+1} = \bar{x}_j + \bar{\alpha}_j \bar{p}_j + \xi_{j+1}^{\bar{x}}, \quad \bar{r}_{j+1} = \bar{r}_j - \bar{\alpha}_j A \bar{p}_j + \xi_{j+1}^{\bar{r}},$$

where  $\xi_{j+1}^{\bar{x}}$  and  $\xi_{j+1}^{\bar{r}}$  represent local rounding errors, and where  $\bar{s}_j = A \bar{p}_j$ . We refer to the analysis in [6, 12] for bounds on the norms of these local rounding errors. It follows directly from (32) that in classic CG the residual gap is

$$(33) \quad \bar{\mathbf{r}}_{j+1} - \bar{r}_{j+1} = (b - A \bar{x}_{j+1}) - \bar{r}_{j+1} = \bar{\mathbf{r}}_j - \bar{r}_j - A \xi_{j+1}^{\bar{x}} - \xi_{j+1}^{\bar{r}} = \bar{\mathbf{r}}_0 - \bar{r}_0 - \sum_{k=0}^j (A \xi_{k+1}^{\bar{x}} + \xi_{k+1}^{\bar{r}}).$$

In each iteration local rounding errors of the form  $A \xi_{j+1}^{\bar{x}} + \xi_{j+1}^{\bar{r}}$  add to the gap on the residual. Thus, local rounding errors are merely accumulated in the classic CG algorithm, and no amplification of rounding errors occurs. To avoid confusion we stress that (32)-(33) apply to classic CG only.

We now turn towards analyzing the p( $l$ )-CG method in a finite precision framework. Consider the faulty variant of recurrence relation (26) for  $\bar{x}_j$  in p( $l$ )-CG, Alg. 2, in finite precision:

$$(34) \quad \bar{x}_j = \bar{x}_{j-1} + \bar{\zeta}_{j-1} \bar{p}_{j-1} + \xi_j^{\bar{x}} = \bar{x}_0 + \bar{P}_j \bar{q}_j + \Theta_j^{\bar{x}} \mathbf{1},$$

where  $\bar{q}_j = (\bar{\zeta}_0, \dots, \bar{\zeta}_{j-1})^T$  is characterized by the entries  $\bar{\zeta}_j$  which are computed explicitly in Alg. 2,  $\Theta_j^{\bar{x}} = [\xi_1^{\bar{x}}, \xi_1^{\bar{x}}, \dots, \xi_j^{\bar{x}}]$  with  $\|\xi_j^{\bar{x}}\| \leq (\|\bar{x}_{j-1}\| + 2 \|\bar{\zeta}_{j-1}\| \|\bar{p}_{j-1}\|) \epsilon$  are local rounding errors, and  $\mathbf{1} = [1, 1, \dots, 1]^T$ . Similarly, the finite precision recurrence relation for  $\bar{p}_j$  in Alg. 2 is

$$(35) \quad \bar{p}_j = (\bar{v}_j - \bar{\delta}_{j-1} \bar{p}_{j-1}) / \bar{\eta}_j + \xi_j^{\bar{p}} \quad \Leftrightarrow \quad \bar{V}_{j+1} = \bar{P}_{j+1} \bar{U}_{j+1} + \Theta_{j+1}^{\bar{p}},$$

where  $\bar{U}_j$  is the upper triangular factor of  $\bar{T}_{j,j} = \bar{L}_j \bar{U}_j$  and  $\Theta_{j+1}^{\bar{p}} = -[\bar{\eta}_0 \xi_0^{\bar{p}}, \bar{\eta}_1 \xi_1^{\bar{p}}, \dots, \bar{\eta}_j \xi_j^{\bar{p}}]$  with  $\|\xi_j^{\bar{p}}\| \leq (2/\bar{\eta}_j \|\bar{v}_{j-1}\| + 3 \|\bar{\delta}_{j-1}\|/\bar{\eta}_j \|\bar{p}_{j-1}\|) \epsilon$  are local rounding errors.

Substitution of expression (35), i.e.  $\bar{P}_j = (\bar{V}_j - \Theta_j^{\bar{p}}) \bar{U}_j^{-1}$ , into equation (34) yields

$$(36) \quad \bar{x}_j = \bar{x}_0 + \bar{V}_j \bar{U}_j^{-1} \bar{q}_j - \Theta_j^{\bar{p}} \bar{U}_j^{-1} \bar{q}_j + \Theta_j^{\bar{x}} \mathbf{1}.$$

Consequently, the actual residual  $\bar{\mathbf{r}}_j$  can be written as

$$(37) \quad \bar{\mathbf{r}}_j = b - A \bar{x}_j = \bar{\mathbf{r}}_0 - A \bar{V}_j \bar{U}_j^{-1} \bar{q}_j + A \Theta_j^{\bar{p}} \bar{U}_j^{-1} \bar{q}_j - A \Theta_j^{\bar{x}} \mathbf{1}.$$

In this expression the computed basis vectors  $\bar{v}_j$  are calculated from the finite precision variant of the recurrence relation (17), i.e.

$$(38) \quad \bar{v}_{j+1} = \left( \bar{z}_{j+1} - \sum_{k=j-2l+1}^j \bar{g}_{k,j+1} \bar{v}_k \right) / \bar{g}_{j+1,j+1} + \xi_{j+1}^{\bar{v}}, \quad 0 \leq j < i - l,$$

where the size of the local rounding errors  $\xi_{j+1}^{\bar{v}}$  can be bounded in terms of the machine precision  $\epsilon$  as  $\|\xi_{j+1}^{\bar{v}}\| \leq (2\|\bar{z}_{j+1}\|/|\bar{g}_{j+1,j+1}| + 3\sum_{k=j-2l+1}^j |\bar{g}_{k,j+1}|/|\bar{g}_{j+1,j+1}| \|\bar{v}_k\|)\epsilon$ . On the other hand, for any  $j \geq 0$  the actual basis vector  $\bar{\mathbf{v}}_{j+1}$  satisfies the Lanczos relation exactly, that is, it is defined as

$$(39) \quad \bar{\mathbf{v}}_{j+1} = (A\bar{v}_j - \bar{\gamma}_j\bar{v}_j - \bar{\delta}_{j-1}\bar{v}_{j-1})/\bar{\delta}_j, \quad 0 \leq j < i-l.$$

For  $j = 0$  it is assumed that  $\bar{v}_{-1} = 0$ . By subtracting the computed basis vector  $\bar{v}_{j+1}$  from both sides of the equation (39), it is easy to see that this relation alternatively translates to

$$A\bar{v}_j = \bar{\delta}_{j-1}\bar{v}_{j-1} + \bar{\gamma}_j\bar{v}_j + \bar{\delta}_j\bar{v}_{j+1} + \bar{\delta}_j(\bar{\mathbf{v}}_{j+1} - \bar{v}_{j+1}), \quad 0 \leq j < i-l$$

or written in matrix notation:

$$(40) \quad A\bar{V}_j = \bar{V}_{j+1}\bar{T}_{j+1,j} + (\bar{\mathbf{V}}_{j+1} - \bar{V}_{j+1})\bar{\Delta}_{j+1,j}, \quad 1 \leq j \leq i-l,$$

where  $\bar{\Delta}_{j+1,j}$  is

$$\bar{\Delta}_{j+1,j} = \begin{pmatrix} 0 & & & & \\ \bar{\delta}_0 & 0 & & & \\ & \bar{\delta}_1 & 0 & & \\ & & \ddots & & 0 \\ & & & \bar{\delta}_{j-1} & \end{pmatrix}.$$

We call  $\bar{\mathbf{V}}_{j+1} - \bar{V}_{j+1}$  the ‘gaps’ on the computed basis vectors, in analogy to the residual gaps. Expression (40) enables to further work out the expression (37) for the actual residual as follows:

$$(41) \quad \begin{aligned} \bar{\mathbf{r}}_j &= \bar{\mathbf{r}}_0 - \bar{V}_{j+1}\bar{T}_{j+1,j}\bar{U}_j^{-1}\bar{q}_j + (\bar{\mathbf{V}}_{j+1} - \bar{V}_{j+1})\bar{\Delta}_{j+1,j}\bar{U}_j^{-1}\bar{q}_j + A\Theta_j^{\bar{p}}\bar{U}_j^{-1}\bar{q}_j - A\Theta_j^{\bar{x}}\mathbf{1} \\ &= \bar{r}_j + (\bar{\mathbf{r}}_0 - \bar{r}_0) - (\bar{\mathbf{V}}_{j+1} - \bar{V}_{j+1})\bar{\Delta}_{j+1,j}\bar{U}_j^{-1}\bar{q}_j + A\Theta_j^{\bar{p}}\bar{U}_j^{-1}\bar{q}_j - A\Theta_j^{\bar{x}}\mathbf{1} \end{aligned}$$

where the implicitly computed residual  $\bar{r}_j$  corresponds to the residual norm  $\|\bar{r}_j\| = |\bar{\zeta}_j|$ , see Theorem 9; it is defined as

$$(42) \quad \bar{r}_j = \bar{r}_0 - \bar{V}_{j+1}\bar{T}_{j+1,j}\bar{U}_j^{-1}\bar{q}_j = -\bar{\delta}_{j-1}(e_j^T\bar{U}_j^{-1}\bar{q}_j)\bar{v}_j = \bar{\zeta}_j\bar{v}_j.$$

Expression (41) indicates that the gap between  $\bar{\mathbf{r}}_j$  and  $\bar{r}_j$  critically depends on the basis vector gaps  $\bar{\mathbf{V}}_{j+1} - \bar{V}_{j+1}$ . We therefore proceed by analyzing the gap on the basis vectors in p( $l$ )-CG.

By setting  $\Theta_j^{\bar{v}} = [\theta_0^{\bar{v}}, \theta_1^{\bar{v}}, \dots, \theta_{j-1}^{\bar{v}}] := [0, \bar{g}_{1,1}\xi_1^{\bar{v}}, \dots, \bar{g}_{j-1,j-1}\xi_{j-1}^{\bar{v}}]$ , we obtain from (38) the matrix expression

$$(43) \quad \bar{Z}_j = \bar{V}_j\bar{G}_j + \Theta_j^{\bar{v}}, \quad 1 \leq j \leq i-l.$$

The computed auxiliary basis vector  $\bar{z}_{j+1}$  satisfies a finite precision version of the recurrence relation (13), which pours down to

$$(44) \quad \bar{z}_{j+1} = \begin{cases} (A - \sigma_j I)\bar{z}_j + \xi_{j+1}^{\bar{z}}, & 0 \leq j < l \\ (A\bar{z}_j - \bar{\gamma}_{j-l}\bar{z}_j - \bar{\delta}_{j-l-1}\bar{z}_{j-1})/\bar{\delta}_{j-l} + \xi_{j+1}^{\bar{z}}, & l \leq j < i, \end{cases}$$

where the local rounding errors  $\xi_{j+1}^{\bar{z}}$  are bounded by

$$\|\xi_{j+1}^{\bar{z}}\| \leq \begin{cases} \mu\sqrt{n}\|A - \sigma_j I\|\|\bar{z}_j\|\epsilon, & 0 \leq j < l, \\ \left( (\mu\sqrt{n} + 2)\frac{\|A\|}{|\bar{\delta}_{j-l}|}\|\bar{z}_j\| + 3\frac{|\bar{\gamma}_{j-l}|}{|\bar{\delta}_{j-l}|}\|\bar{z}_j\| + 3\frac{|\bar{\delta}_{j-l-1}|}{|\bar{\delta}_{j-l}|}\|\bar{z}_{j-1}\| \right)\epsilon, & l \leq j < i. \end{cases}$$

Here  $n$  is the number of rows/columns in the matrix  $A$  and  $\mu$  is the maximum number of non-zeros over all rows of  $A$ . Expression (44) can be summarized in matrix notation as:

$$(45) \quad A\bar{Z}_j = \bar{Z}_{j+1}\bar{B}_{j+1,j} + \Theta_j^{\bar{z}}, \quad 1 \leq j \leq i,$$

where  $\Theta_j^{\bar{z}} = [\theta_0^{\bar{z}}, \theta_1^{\bar{z}}, \dots, \theta_{j-1}^{\bar{z}}]$ , with  $\theta_k^{\bar{z}} = \xi_{k+1}^{\bar{z}}$  for  $0 \leq k < l$  and  $\theta_k^{\bar{z}} = \bar{\delta}_{k-l}\xi_{k+1}^{\bar{z}}$  for  $l \leq k < i$ . Furthermore, the recursive definitions of the scalar coefficients  $\bar{\gamma}_j$  and  $\bar{\delta}_j$  in Alg. 2 imply that in iteration  $i$  the following matrix relations hold:

$$(46) \quad \bar{G}_{j+1}\bar{B}_{j+1,j} = \bar{T}_{j+1,j}\bar{G}_j, \quad 1 \leq j \leq i-l.$$

The gap  $\bar{V}_{j+1} - \bar{V}_{j+1}$  can now be computed by combining the above expressions. It holds that<sup>2</sup>

$$(47) \quad \begin{aligned} \bar{V}_{j+1} - \bar{V}_{j+1} &\stackrel{(40)}{=} (A\bar{V}_j - \bar{V}_{j+1}\bar{T}_{j+1,j})\bar{\Delta}_{j+1,j}^+ \\ &\stackrel{(43)}{=} (A\bar{Z}_j\bar{G}_j^{-1} - \bar{Z}_{j+1}\bar{G}_{j+1}^{-1}\bar{T}_{j+1,j} - A\Theta_j^{\bar{v}}\bar{G}_j^{-1} + \Theta_{j+1}^{\bar{v}}\bar{G}_{j+1}^{-1}\bar{T}_{j+1,j})\bar{\Delta}_{j+1,j}^+ \\ &\stackrel{(46)}{=} (A\bar{Z}_j\bar{G}_j^{-1} - \bar{Z}_{j+1}\bar{B}_{j+1,j}\bar{G}_j^{-1} - A\Theta_j^{\bar{v}}\bar{G}_j^{-1} + \Theta_{j+1}^{\bar{v}}\bar{B}_{j+1,j}\bar{G}_j^{-1})\bar{\Delta}_{j+1,j}^+ \\ &\stackrel{(45)}{=} (\Theta_j^{\bar{z}} - A\Theta_j^{\bar{v}} + \Theta_{j+1}^{\bar{v}}\bar{B}_{j+1,j})\bar{G}_j^{-1}\bar{\Delta}_{j+1,j}^+. \end{aligned}$$

Consequently, it is clear that in  $p(\ell)$ -CG the local rounding errors in  $\Theta_j^{\bar{z}}$ ,  $A\Theta_j^{\bar{v}}$  and  $\Theta_{j+1}^{\bar{v}}\bar{B}_{j+1,j}$  are possibly amplified by the entries of the matrix  $\bar{G}_j^{-1}\bar{\Delta}_{j+1,j}^+$ . This in turn implies an amplification of local rounding errors in expression (41), leading to reduced maximal attainable accuracy. Since  $\bar{\Delta}_{j+1,j}^+$  is a diagonal matrix, the propagation of local rounding errors in  $p(\ell)$ -CG is primarily governed by the inverse of the (finite precision variant of the) basis transformation matrix  $\bar{G}_j$ .

**4.2. Bounding the basis vector gaps in finite precision  $p(\ell)$ -CG.** As the matrix  $\bar{G}_j^{-1}$  fulfills a crucial role in the propagation of local rounding errors in  $p(\ell)$ -CG, see (47), we aim to establish bounds on the maximum norm of  $\bar{G}_j^{-1}$  in this section. Consider the norm

$$(48) \quad \|\bar{G}_j^{-1}\|_{\max} = \max_{k,l} |\bar{G}_j^{-1}(k,l)|,$$

which characterizes the propagation of local rounding errors in the  $\bar{V}_j$  basis in  $p(\ell)$ -CG. When the maximum norm is larger than one local rounding errors may be amplified, see expression (47).

The inverse of the banded matrix  $\bar{G}_j$  is an upper triangular matrix, which can be expressed as

$$(49) \quad \bar{G}_j^{-1} = \sum_{k=0}^{j-1} \left( -\bar{\Lambda}_j^{-1}\bar{G}_j^{\Delta} \right)^k \bar{\Lambda}_j^{-1},$$

where  $\bar{\Lambda}_j := [\delta_{mk}\bar{g}_{m,k}]$  contains the diagonal of  $\bar{G}_j$  and  $\bar{G}_j^{\Delta} := \bar{G}_j - \bar{\Lambda}_j$  is the strictly upper triangular part of  $\bar{G}_j$ .

LEMMA 15. *Assume  $1 \leq j \leq i-l+1$  such that the basis  $\bar{V}_j$  is orthonormal. Let the Krylov subspace basis transformation matrix  $\bar{G}_j$  be defined by  $\bar{G}_j = \bar{V}_j^T \bar{Z}_j + \bar{V}_j^T \Theta_j^{\bar{v}}$  for  $1 \leq j \leq i-l+1$  as in (43). Then it holds that*

$$(50) \quad \|\bar{G}_j\|_{\max} \leq \|P_l(A)\| + \|\xi_k^{\bar{z}}\| + \|\theta_k^{\bar{v}}\|.$$

<sup>2</sup>Note that the Moore-Penrose (left) pseudo-inverse  $\bar{\Delta}_{j+1,j}^+ = (\bar{\Delta}_{j+1,j}^* \bar{\Delta}_{j+1,j})^{-1} \bar{\Delta}_{j+1,j}^*$  of the lower diagonal matrix  $\bar{\Delta}_{j+1,j}$  in expression (47) is an upper diagonal matrix, where  $\bar{\Delta}_{j+1,j}^*$  is its Hermitian transpose.

*Proof.* Since for any  $0 \leq m \leq i - l$  the vector  $\bar{v}_m$  is normalized, i.e.  $\|\bar{v}_m\| = 1$ , the following bound on the entries of  $\bar{G}_j$  holds:

$$(51) \quad \begin{aligned} |\bar{g}_{m,k}| &= |(\bar{z}_k, \bar{v}_m) - (\theta_k^{\bar{v}}, \bar{v}_m)| \leq \|\bar{z}_k\| + \|\theta_k^{\bar{v}}\| \leq \|P_l(A)\bar{v}_{k-l} + \xi_k^{\bar{z}}\| + \|\theta_k^{\bar{v}}\| \\ &\leq \|P_l(A)\| + \|\xi_k^{\bar{z}}\| + \|\theta_k^{\bar{v}}\|, \end{aligned} \quad 0 \leq m \leq i - l, \quad 0 \leq k \leq i. \quad \square$$

We remark that the matrix  $\bar{G}_j$  is not necessarily diagonally dominant, since the norms  $\|\bar{z}_k\|$  are not guaranteed to be monotonically decreasing in p( $l$ )-CG. Consequently, if the bound in (50) is tight, Lemma 15 suggests that when  $\|P_l(A)\|$  is large,  $\|\bar{G}_j^{-1}\|_{\max}$  may be (much) larger than one. This observation leads to some interesting insights. First, note that the norm  $\|\bar{G}_j\|_{\max}$  increases monotonically with respect to the iteration index  $j$ , since each iteration adds a new column to  $\bar{G}_j$ . Furthermore, an increase in  $j$  also implies an increase in the number of terms in the summation in (49). The norm  $\|\bar{G}_j^{-1}\|_{\max}$  thus increases as a function of  $j$ . Secondly, an increasing pipeline length  $l$  increases the number of non-zero diagonals in  $\bar{G}_j$  significantly, see Lemma 5 and Appendix 6, which impacts the norm of the right-hand side expression in (49). The pipeline length  $l$  also relates directly to the norm  $\|P_l(A)\|$  which bounds the norm  $\|\bar{G}_j\|_{\max}$  in (50). Therefore, it is expected that  $\|\bar{G}_j^{-1}\|_{\max}$  grows as a function of  $l$  and the p( $l$ )-CG method will attain a less accurate maximal attainable precision with increasing  $l$ , see Fig. 1. Finally, remark that it was also illustrated by Fig. 1 that the choice of the shifts  $\{\sigma_0, \dots, \sigma_{l-1}\}$  has a significant impact on the numerical stability of the p( $l$ )-CG method. A sub-optimal choice for the shifts may lead to a significant increase in the norm of the polynomial,  $\|P_l(A)\|$ , which bounds the propagation of local rounding errors in p( $l$ )-CG, see Lemma 15. The ‘optimal’ shifts  $\sigma_i$  ( $0 \leq i < l$ ) are the roots of the degree  $l$  Chebyshev polynomial, see (8), which minimize the 2-norm of  $P_l(A)$ , see [30, 21].

**5. Experimental results.** Parallel performance measurements in this section result from a PETSc [3] implementation of p( $l$ )-CG on a distributed memory machine using the message passing paradigm (MPI). The p( $l$ )-CG method is validated on a two-dimensional Laplacian PDE model with homogeneous Dirichlet boundary conditions, discretized using second order finite differences on a uniform  $n = n_x \times n_y$  point discretization of the unit square. The resulting 5-point stencil Poisson problem forms the basis for many HPC applications to which the pipelined CG method can be applied. The conditioning of these types of systems is typically bad for large problem sizes, implying that iterative solution using Krylov subspace methods is non-trivial. Note that vectors are distributed uniformly across the number of available workers and stored locally (distributed memory). This implies that the matrix is partitioned by contiguous chunks of rows across processors (which is the default way in which PETSc partitions matrix operators).

### 5.1. Parallel performance.

*Test setup 1.* The first parallel strong scaling experiment is performed on a small cluster with 20 compute nodes, consisting of two 6-core Intel Xeon X5660 Nehalem 2.80 GHz processors each (12 cores per node). Nodes are connected by  $4 \times$  QDR InfiniBand technology (32 Gb/s point-to-point bandwidth). We use PETSc version 3.6.3 [3]. The MPI library used for this experiment is MPICH-3.1.3<sup>3</sup>. The PETSc environment variables `MPICH_ASYNC_PROGRESS=1` and `MPICH_MAX_THREAD_SAFETY=multiple` are set to ensure optimal parallelism by allowing for non-blocking global communication, see Section 3.1. A 2D Poisson type linear system with exact solution  $\hat{x}_j = 1$  and right-hand side  $b = A\hat{x}$  is solved, and the initial guess is chosen to be  $\bar{x}_0 = 0$ . This benchmark problem is available in the PETSc distribution as example 2 in the Krylov subspace

<sup>3</sup><http://www.mpich.org/>

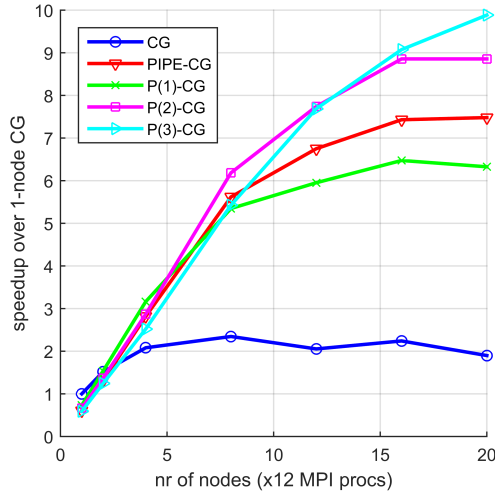


FIG. 3. Strong scaling experiment on up to 20 nodes (240 processes) for a 5-point stencil 2D Poisson problem with 1,000,000 unknowns. Speedup over single-node classic CG for various pipeline lengths. All methods converged to  $\|\bar{r}_i\|_2/\|b\|_2 = 1.0e-5$  in 1342 iterations.

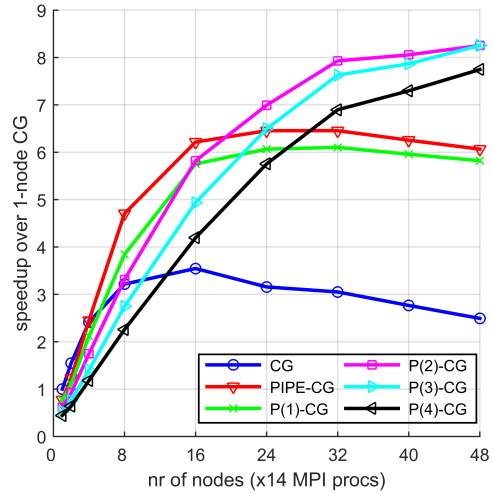


FIG. 4. Strong scaling experiment on up to 48 nodes (672 processes) for a 5-point stencil 2D Poisson problem with 3,062,500 unknowns. Speedup over single-node classic CG for various pipeline lengths. All methods performed 1500 iterations with  $\|\bar{r}_i\|_2/\|b\|_2 = 6.3e-4$ .

solvers (KSP) folder. The simulation domain is discretized using  $1000 \times 1000$  grid points (1 million unknowns). No preconditioner is applied in this experiment. The tolerance imposed on the scaled recursive residual norm  $\|\bar{r}_i\|_2/\|b\|_2$  is  $10^{-5}$ . For  $p(l)$ -CG stabilizing Chebyshev shifts are used based on the interval  $[\lambda_{\min}, \lambda_{\max}] = [0, 8]$ , see Remark 3.

Fig. 3 shows the speedup of CG, p-CG and  $p(l)$ -CG (for different values of  $l$ ) over CG on one node. Timings reported are the most favorable results (in the sense of smallest overall run-time) over 5 individual runs of each method. All methods perform the same number of iterations to reach the preset tolerance. For small numbers of nodes pipelined methods are typically slower than classic CG due to the computational overhead in the initial  $l$  iterations and the extra vector operations in the basis vector recurrences. For large numbers of nodes pipelined methods outperform classic CG, for which speedup stagnates from 4 nodes onward on this problem setup. The p-CG method [25] tends to scale slightly better than the p(1)-CG variant. Scaling of length one pipelined variants also inevitably stagnates from a certain number of nodes onward. The  $p(l)$ -CG methods with deeper pipelines ( $l = 2, 3$ ) continue to scale beyond the stagnation point of p(1)-CG. The attainable speedup of p(3)-CG on 20 nodes over classic CG on 20 nodes is roughly  $5\times$ , whereas the p(1)-CG method on 20 nodes is approximately  $3\times$  faster than classic CG on the same number of nodes. The theoretical maximum speedup of  $p(l)$ -CG over CG is  $t(\text{SPMV} + 2 \text{ GLRED}) / \max(t(\text{SPMV}), t(\text{GLRED}))/l$  where  $t(\text{SPMV})$  is the time to apply the matrix (and preconditioner) and  $t(\text{GLRED})$  is the time of one global reduction phase, see Table 1. This model neglects the time spent in local operations and thus holds only on large numbers of nodes. In the ideal  $p(l)$ -CG scenario when  $t(\text{GLRED}) = lt(\text{SPMV})$ , the model suggests that the maximal speedup of  $p(l)$ -CG over CG is a factor  $(2l + 1)\times$ .

*Test setup 2.* A strong scaling experiment on a different hardware setup is shown in Fig. 4. Here a medium-sized cluster with 48 compute nodes consisting of two 14-core Intel E5-2680v4 Broadwell

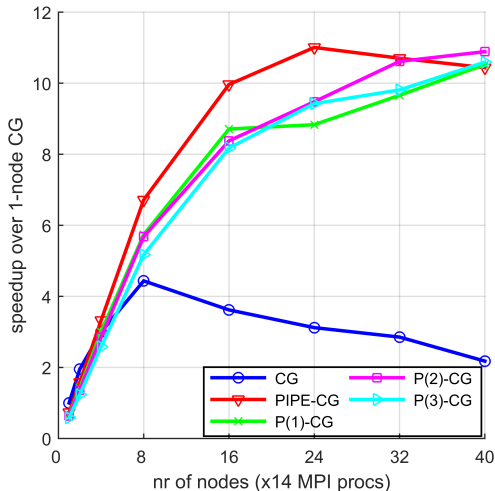


FIG. 5. Strong scaling experiment on up to 40 nodes (560 processes) for a block Jacobi preconditioned 2D Poisson problem with 3,062,500 unknowns. All methods performed 600 iterations with  $\|\bar{r}_i\|_2/\|b\|_2 = 1.8e-4$  (on 1 node) and  $\|\bar{r}_i\|_2/\|b\|_2 \leq 9.3e-4$  (on 40 nodes).

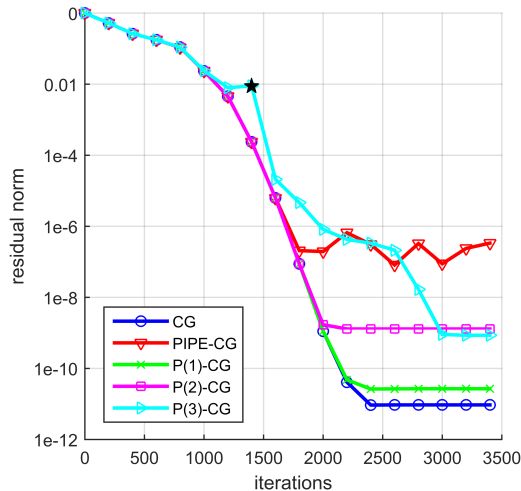


FIG. 6. Accuracy experiment on 20 nodes (240 processes) for a 5-point stencil 2D Poisson problem with 1,000,000 unknowns. Residual norm  $\|b - A\bar{x}_i\|_2$  as a function of time spent by the algorithm. Minimal/maximal number of iterations is 200/3400 for all methods.

generation CPUs connected through an EDR InfiniBand network is used. PETSc version 3.7.6 and MPICH-3.3a2 are installed on the machine. A  $1750 \times 1750$  2D Poisson type linear system with right-hand side  $b = A\hat{x}$ , where  $\hat{x}_j = 1$ , is solved on this system. The outcome of the scaling experiment is shown in Fig. 4. The number of iterations was capped at 1500 for this problem, which is equivalent to a relative residual norm tolerance of  $6.3e-4$ . Similar observations as for Fig. 3 can be made; the achievable parallel performance gain by using longer pipelines is apparent from the experiment. However, the balance between time spent in communication vs. computation is clearly different from the experiment reported in Fig. 3. Note that on this problem for pipeline lengths  $l \geq 4$  the computational overhead of the initial  $l$  start-up iterations (in which the pipeline is filled) and the additional AXPY operations required for the basis vector recurrences slow down the algorithm significantly. Hence, on up to 48 nodes the  $p(l)$ -CG algorithm with  $l = 2, 3$  slightly outperforms the  $p(l)$ -CG algorithm with  $l \geq 4$ . Deeper pipelined  $p(l)$ -CG ( $l \geq 4$ ) methods are expected to eventually scale further, achieving even better speedups beyond the number of nodes reported here.

**5.2. Preconditioning.** Fig. 5 shows another parallel performance experiment in the setting of *Test setup 2*. Contrary to Fig. 4, here a preconditioner is included and Alg. 2 is applied to solve the preconditioned system, see Section 2.3 for details. The preconditioner is a simple block Jacobi scheme, supplied to PETSc by the argument `-pc_type bjacobi`, where the local blocks are approximately inverted using ILU. Its straightforward parallelism makes block Jacobi an ideal preconditioner for pipelined methods, although the convergence benefit of this preconditioner may deteriorate slightly as the number of nodes increases. For preconditioned  $p(l)$ -CG Chebyshev shifts based on the interval  $[\lambda_{\min}, \lambda_{\max}] = [0, 1.5]$  are used, cf. Remark 3. After 600 iterations a relative residual accuracy  $\|\bar{r}_i\|_2/\|b\|_2 \leq 1e-3$  is reached for all methods and node numbers. On 40 nodes the

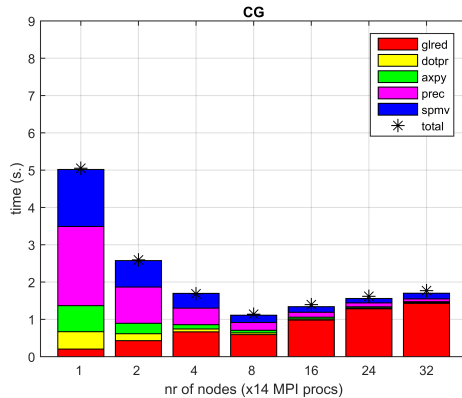


FIG. 7. Detailed timing breakdown of the classic CG algorithm for the 3.062.500 unknowns 2D Poisson strong scaling experiment in Fig. 5 on up to 32 nodes.

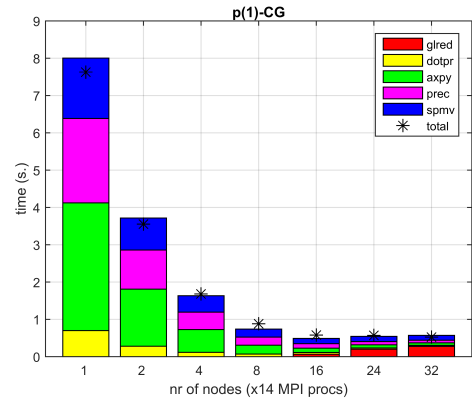


FIG. 8. Detailed timing breakdown of the p(1)-CG algorithm for the 3.062.500 unknowns 2D Poisson strong scaling experiment in Fig. 5 on up to 32 nodes.

pipelined methods all show comparable speedups over classic CG. The p(2)-CG method outperforms p(1)-CG by a small fraction on 40 nodes. Compared to the unpreconditioned experiments reported in Fig. 4 the performance gains of using longer pipelines are rather limited here. This can be understood by considering the balance between time spent in computations vs. communication. Figs. 7-8 give a detailed overview of the time spent in each phase for the CG and p(1)-CG methods respectively. In Fig. 8 the ‘GLRED’ bar represents the part of the global communication phase that is not overlapped with the SPMV and preconditioner. It is clear from Fig. 8 that on up to 32 nodes there is no more time to gain from overlapping the communication phase with more than one SPMV and preconditioner application, and hence for this problem setup the additional speedup achievable by using pipelines with  $l > 1$  compared to p(1)-CG is expected to be small, as illustrated in Fig. 5.

**5.3. Numerical accuracy.** Fig. 6 presents an accuracy experiment for *Test setup 1*. The actual residual 2-norm  $\|b - A\bar{x}_i\|_2$  is shown as a function of iterations. Fig. 6 indicates that the maximal attainable accuracy of the p( $l$ )-CG method decreases with growing pipeline lengths  $l$ . It was analyzed in [12, 6] that the attainable accuracy of p-CG can be significantly worse compared to classic CG due to the propagation of local rounding errors in the vector recurrences. Whereas it is clear from the figure that the maximal attainable accuracy for p(2)-CG is worse than for p(1)-CG, the latter appears to be more robust to rounding errors compared to the length one pipelined p-CG method from [25]. We again point out that the p-CG and p( $l$ )-CG methods are essentially different algorithms as stated in Remark 10. Note that the p(3)-CG method encounters a square root breakdown in iteration 1393 (Fig. 6, ★) and consequently performs a restart. Due to the restart the accuracy attainable by p(3)-CG and p(2)-CG is comparable; however, the number of iterations required to reach it is considerably higher for p(3)-CG. Supplementary and insightful numerical experiments on maximal attainable accuracy for a variety of SPD matrices from the Matrix Market collection (<http://math.nist.gov/MatrixMarket/>) can be found in Table 2 in Appendix D.

We now present numerical experiments regarding the numerical analysis of the p( $l$ )-CG method discussed in Section 4. Consider the  $200 \times 200$  discretized 2D Poisson problem on  $[0, 1]^2$  for illustration purposes in this remainder of this section. The right-hand side is  $b = A\hat{x}$  with  $\hat{x} = 1/\sqrt{n}$ , unless explicitly stated otherwise. This relatively simple problem is severely ill-conditioned and

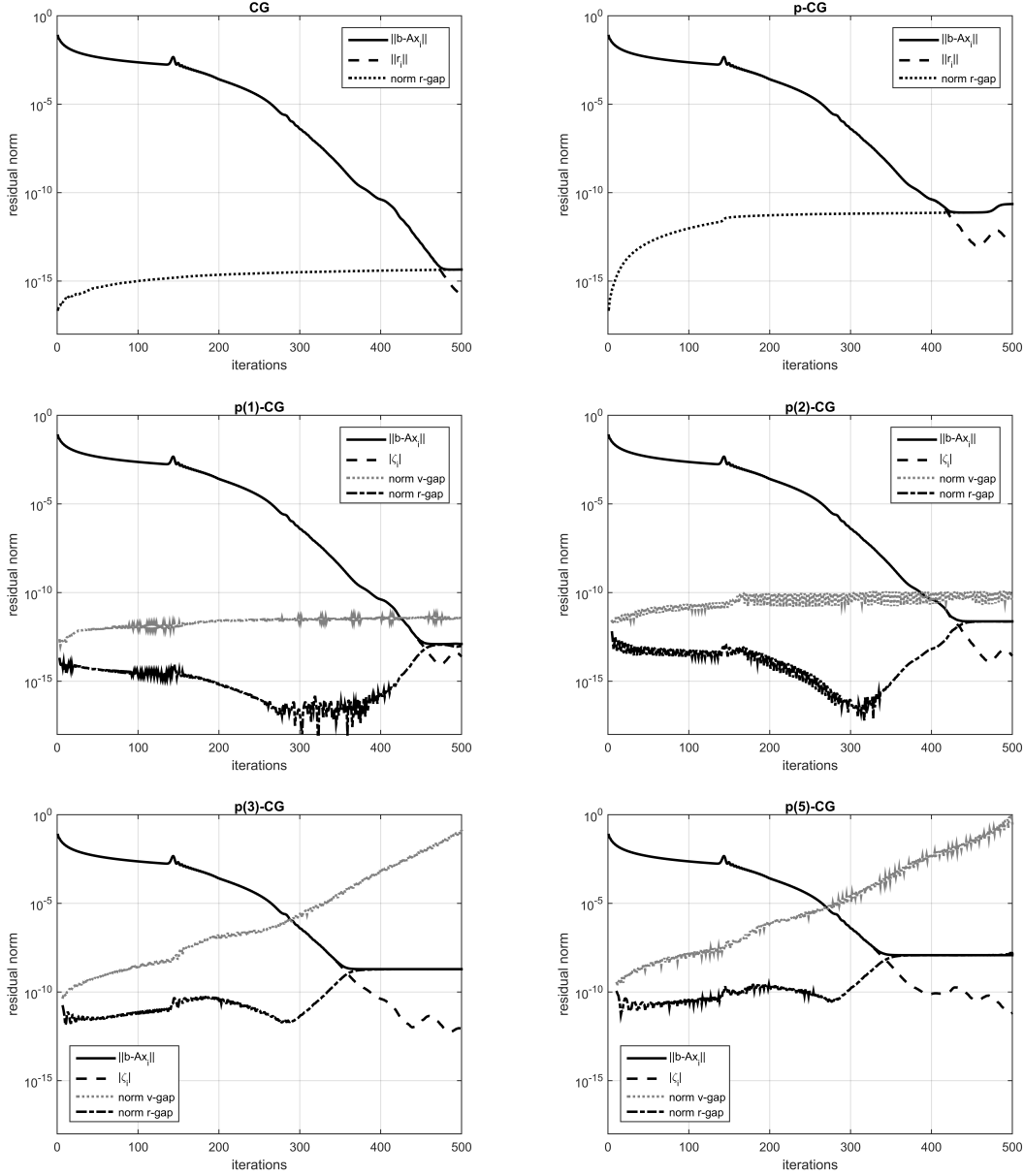


FIG. 9. Actual residual norm  $\|b - A\bar{x}_{j+1}\|$ , recursively computed residual norm  $\|\bar{r}_{j+1}\|$ , basis gap norm  $\|\bar{\mathbf{v}}_{j+1} - \bar{v}_{j+1}\|$  and residual gap norm  $\|\bar{\mathbf{F}}_{j+1} - \bar{r}_{j+1}\|$  for different CG variants on a 2D Poisson problem with  $200 \times 200$  unknowns corresponding to Fig. 1 (left). For CG and p-CG (top) the norm of the residual gap  $(b - A\bar{x}_{j+1}) - \bar{r}_{j+1}$  is displayed, where  $\bar{r}_{j+1}$  is computed using (32). For  $p(\ell)$ -CG with  $\ell = 1, 2, 3, 5$  (middle and bottom) the norms of the gaps  $\bar{\mathbf{v}}_{j-l+1} - \bar{v}_{j-l+1}$  and  $\bar{\mathbf{F}}_{j-l+1} - \bar{r}_{j-l+1}$  are shown, where  $\bar{\mathbf{v}}_{j-l+1}$  satisfies (39),  $\bar{v}_{j-l+1}$  is computed using the recurrence (38) and  $\bar{\mathbf{F}}_{j-l+1} - \bar{r}_{j-l+1}$  is defined by (41) using  $\bar{\mathbf{v}}_{j-l+1}$  and  $\bar{v}_{j-l+1}$ .

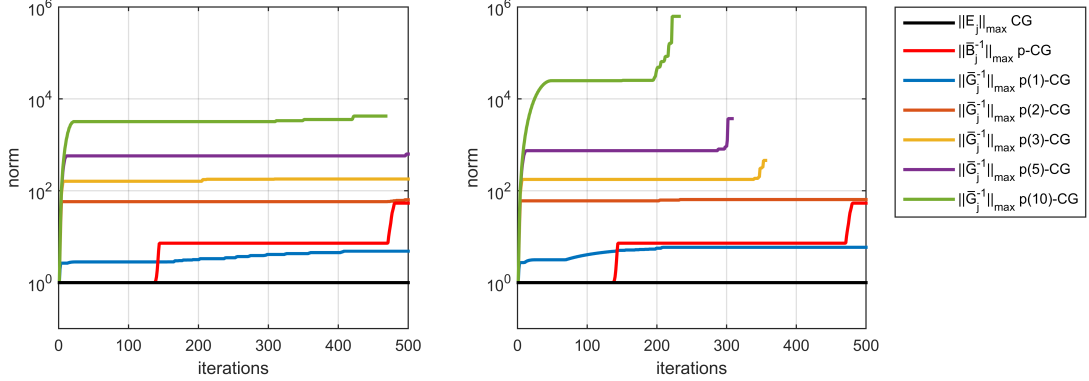


FIG. 10. Maximum norms of the essential matrices  $E_j$ ,  $\bar{B}_j^{-1}$  and  $\bar{G}_j^{-1}$  involved in the local rounding error propagation for different variants of CG. See expression (33) for CG and reference [12] for p-CG. See also Appendix 6 for definitions of the matrices  $E_j$  and  $\bar{B}_j^{-1}$  that govern the residual gaps for CG and p-CG respectively. See expressions (41) and (47) for details on the residual gap in p( $\ell$ )-CG. Left: with optimal Chebyshev shifts on the interval  $[0,8]$ , cf. Fig. 1 (left). Right: with sub-optimal Chebyshev shifts on the interval  $[0,8*1.005]$ , cf. Fig. 1 (right).

serves as an adequate tool to demonstrate the rounding error analysis from Section 4.

Fig. 9 shows the norms of the actual residual  $\bar{\mathbf{r}}_j = b - A\bar{x}_j$  and computed residual  $\bar{r}_j$  for various CG variants. The norm  $\|\bar{r}_j\|$  is computed as  $|\zeta_j|$  in p( $\ell$ )-CG, see Theorem 9. The figure also displays the norm of the residual gap  $(b - A\bar{x}_j) - \bar{r}_j$  for all methods, see expressions (33) and (41), and the norm of the gap  $\bar{\mathbf{v}}_j - \bar{v}_j$  on the basis for p( $\ell$ )-CG, see (47). For p( $\ell$ )-CG the gap between  $\bar{\mathbf{v}}_j$  and  $\bar{v}_j$  increases dramatically as the iteration proceeds, particularly for large values of  $\ell$ , leading to significantly reduced maximal attainable accuracy as indicated by the related residual gap norms. Note that the residual gaps are not guaranteed to be monotonically increasing. The term  $\|(\bar{\mathbf{V}}_{j+1} - \bar{V}_{j+1})\bar{\Delta}_{j+1,j}\bar{U}_j^{-1}\bar{q}_j\|$  in expression (41) does not necessarily increase, as error gaps on  $\bar{v}_j$  may be averaged out by the linear combination. The following residuals norms  $\|b - A\bar{x}_j\|$  are attained after 500 iterations: 4.47e-15 (CG), 2.28e-11 (p-CG), 1.27e-13 (p(1)-CG), 2.37e-12 (p(2)-CG), 1.94e-09 (p(3)-CG), 1.19e-08 (p(5)-CG).

In Fig. 10 the maximum norm  $\|\bar{G}_j^{-1}\|_{\max}$  is shown as a function of the iteration  $j$  for different pipeline lengths  $l$ . The maximum norms  $\|E_j\|_{\max}$  for CG, see (33), and  $\|\bar{B}_j^{-1}\|_{\max}$  for p-CG, see [12], are also displayed as a reference, see also Appendix 6 for more details. The impact of increasing pipeline lengths on numerical stability is clear from the figure. A comparison between the left panel (optimal shifts) and the right panel (sub-optimal shifts) in Fig. 10 illustrates the influence of the basis choice on the norm of  $\bar{G}_j^{-1}$ , see Section 4.2. No data is plotted when the matrix  $\bar{G}_j$  becomes numerically singular, which corresponds to iterations in which a square root breakdown occurs, see Fig. 1. Relating Fig. 10 to the corresponding convergence histories in Fig. 1, it is clear that the maximal attainable accuracy for p-CG is comparable to that of p(2)-CG, whereas the p(1)-CG algorithm is able to attain a better final precision. The final accuracy level at which the residual stagnates degrades significantly for longer pipelines.

Fig. 11 combines performance and accuracy results of several variants to the CG method into a single figure. The figure shows the relative actual residuals  $\|b - A\bar{x}_j\|/\|b\|$  for the  $750 \times 750$  2D Laplace problem as a function of total time spent by the algorithm. The time spent to compute the

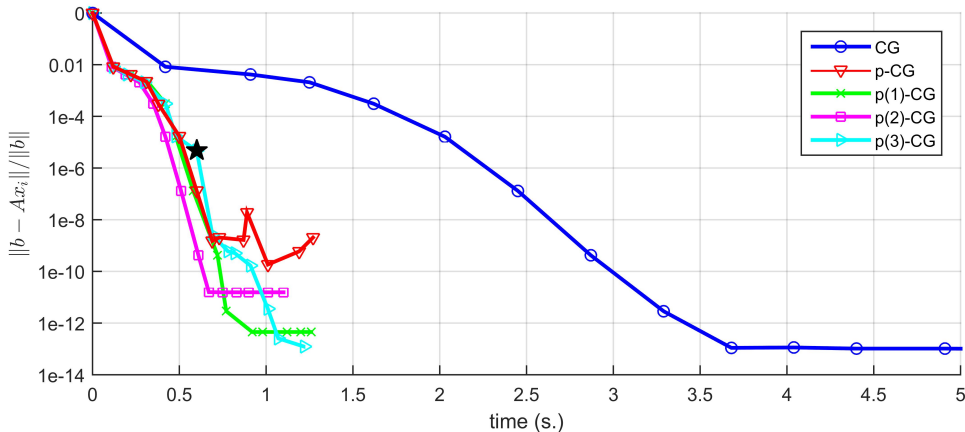


FIG. 11. Performance/accuracy experiment on 10 nodes (120 processes) for a 5-point stencil 2D Poisson problem with 562,500 unknowns. Relative residual norm  $\|b - A\bar{x}_j\|/\|b\|$  as a function of total time spent by the algorithm for various (pipelined) CG variants. Square root breakdown in  $p(3)$ -CG is indicated by the  $\star$  symbol.

actual residuals was not included in the reported timings, since they are in principle not computed in Alg. 2. The experiment is executed on 10 of the nodes specified in *Test setup 1*. The PETSc version used was 3.8.3 in this experiment and communication was performed using Intel MPI 2018.1.163. Similar to the results in Fig. 3-4, the pipelined methods require significantly less overall time compared to classic CG. The  $p(2)$ -CG algorithm outperforms the other CG variants in terms of time to solution, although it cannot reach the same maximal accuracy as the CG or  $p(1)$ -CG methods. Note that  $p(3)$ -CG is able to attain a residual that *does* satisfy  $\|b - A\bar{x}_j\|/\|b\| \leq 1.0e-13$ , whereas  $p(1)$ -CG and  $p(2)$ -CG are not. This is due to the square root breakdown and subsequent restart of the  $p(3)$ -CG algorithm as described in Remark 8. The restart improves final attainable accuracy but delays the algorithm’s convergence compared to other pipelined variants.

**6. Conclusions.** As HPC hardware keeps evolving towards exascale the gap between computational performance and communication latency keeps increasing. Many numerical methods that are historically optimized towards flop performance now need to be revised towards also (or even: primarily) minimizing communication overhead. Several research teams are currently working towards this goal [5, 37, 24, 31, 35], resulting in a variety of communication reducing variants to classic Krylov subspace methods that feature improved scalability on massively parallel hardware.

This work reports on our efforts to extend the communication-hiding pipelined Conjugate Gradient ( $p$ -CG) method to deeper pipelines. The paper derives a variant of CG with deep pipelines, discusses implementation issues, comments on the numerical stability of the algorithm in finite precision, and presents proof-of-concept scaling results. Contrary to the  $p$ -CG method (with pipeline length one) introduced by Ghysels et al. in 2014 [25], the theoretical framework for the  $p(l)$ -CG algorithm is derived starting from the  $p(l)$ -GMRES method [24], rather than the original CG method [33]. The  $p(l)$ -CG method is shown to be a simplification of the  $p(l)$ -GMRES variant from which it was derived in terms of computational and storage costs, which is achieved by exploiting the symmetry of the system matrix and by imposing residual orthogonality.

On massively parallel machines, where the overall solution time is dominated by global reduction

latency, deep pipelined methods outperform the classic CG and p-CG algorithms, as illustrated by the experiments in this work. Initial test results show improved scalability when longer pipelines are used on distributed-multicore hardware. However, contrary to many existing CG method variants [38, 8, 25, 7], the p( $l$ )-CG algorithm may encounter square root breakdowns. Implementation issues and corresponding solutions for the new CG variant are presented, including discussions on overlapping communication latency with computational work and on memory requirements.

It is observed that longer pipelines have an impact on the propagation of local rounding errors and may affect the attainable accuracy on the solution, cf. [6, 12]. This observation is supported by the numerical analysis presented in the manuscript. Practical bounds for the propagation of the local rounding errors are derived, leading to insights into the influence of the pipelined length and the choice of the auxiliary Krylov basis on attainable accuracy. It should be noted that the analysis in this work does not take into account the impact of loss of orthogonality due to rounding error propagation. We also do not expect the analysis to be directly applicable to other pipelined Krylov subspace methods such as p( $\ell$ )-GMRES, although the general approach would likely show resemblances.

In summary, the main result of the paper is to show that it is indeed possible to introduce longer pipelines in the CG algorithm and to give a first experimental verification of the improved scalability. However, the algorithm is rather technical to implement, requires additional storage for the auxiliary variables and features multi-term recurrences that may affect the numerical accuracy. Several directions for future research are suggested by the remarks throughout this manuscript. The robustness of the p( $l$ )-CG method to rounding error propagation and the impact of deeper pipelines on attainable accuracy should be improved in future work. An interesting technique was recently presented by Imberti et al. [35] for  $s$ -step GMRES; however, it remains to be determined whether a similar idea is suitable to ‘stabilize’ p( $l$ )-CG. Finally, although the performance results reported in this work validate the scalability of p( $l$ )-CG for deeper pipelines, it would be interesting to perform large-scale experiments on even bigger parallel systems where very deep pipelines are expected to be even more beneficial, cf. [49] for p( $l$ )-GMRES.

**Acknowledgments.** J. C. acknowledges funding by the University of Antwerp Research Council under the University Research Fund (BOF). S. C. gratefully acknowledges funding by the Flemish Research Foundation (FWO Flanders) under grant 12H4617N. The authors would like to cordially thank Pieter Ghysels (LBNL) for useful comments on previous versions of this manuscript and related discussions on the topic. Additionally, the authors gratefully acknowledge the input of the anonymous referees who aided in optimizing the contents of this paper.

#### REFERENCES

- [1] E. Agullo, S. Cools, L. Giraud, A. Moreau, P. Salas, W. Vanroose, E.F. Yetkin, and M. Zounon. Hard faults and soft-errors: Possible numerical remedies in linear algebra solvers. In *VecPar: International Conference on Vector and Parallel Processing*, pages 11–18. Springer, 2016.
- [2] Z. Bai, J. Demmel, J. Dongarra, A. Ruhe, and H.A. van der Vorst. *Templates for the Solution of Algebraic Eigenvalue Problems: A Practical Guide*. SIAM, 2000.
- [3] S. Balay, S. Abhyankar, M.F. Adams, J. Brown, P. Brune, K. Buschelman, L. Dalcin, V. Eijkhout, W.D. Gropp, D. Kaushik, M.G. Knepley, L. Curfman McInnes, K. Rupp, B.F. Smith, S. Zampini, and H. Zhang. PETSc Web page. <http://www.mcs.anl.gov/petsc>, 2017.
- [4] E. Carson and J. Demmel. A residual replacement strategy for improving the maximum attainable accuracy of  $s$ -step Krylov subspace methods. *SIAM Journal on Matrix Analysis and Applications*, 35(1):22–43, 2014.
- [5] E. Carson, N. Knight, and J. Demmel. Avoiding communication in nonsymmetric Lanczos-based Krylov subspace methods. *SIAM Journal on Scientific Computing*, 35(5):S42–S61, 2013.

- [6] E. Carson, M. Rozložník, Z. Strakoš, P. Tichý, and M. Tůma. The numerical stability analysis of pipelined Conjugate Gradient methods: Historical context and methodology. *The Czech Academy of Sciences, Preprint IM 45-2017*, 2017.
- [7] E.C. Carson. *Communication-avoiding Krylov subspace methods in theory and practice, PhD dissertation*. EECS Department, University of California, Berkeley, 2015.
- [8] A.T. Chronopoulos and C.W. Gear. s-Step iterative methods for symmetric linear systems. *Journal of Computational and Applied Mathematics*, 25(2):153–168, 1989.
- [9] A.T. Chronopoulos and A.B. Kucherov. Block s-step Krylov iterative methods. *Numerical Linear Algebra with Applications*, 17(1):3–15, 2010.
- [10] A.T. Chronopoulos and C.D. Swanson. Parallel iterative s-step methods for unsymmetric linear systems. *Parallel Computing*, 22(5):623–641, 1996.
- [11] S. Cools and W. Vanroose. The communication-hiding pipelined BiCGstab method for the parallel solution of large unsymmetric linear systems. *Parallel Computing*, 65:1–20, 2017.
- [12] S. Cools, E.F. Yetkin, E. Agullo, L. Giraud, and W. Vanroose. Analyzing the effect of local rounding error propagation on the maximal attainable accuracy of the pipelined Conjugate Gradient method. *SIAM Journal on Matrix Analysis and Applications*, 39(1):426–450, 2018.
- [13] E.F. D’Azevedo, V. Eijkhout, and C.H. Romine. Reducing communication costs in the Conjugate Gradient algorithm on distributed memory multiprocessors. Technical report, Technical report, Oak Ridge National Lab, TM/12192, TN, US, 1992.
- [14] E. De Sturler and H.A. Van der Vorst. Reducing the effect of global communication in GMRES(m) and CG on parallel distributed memory computers. *Applied Numerical Mathematics*, 18(4):441–459, 1995.
- [15] J.W. Demmel, M.T. Heath, and H.A. Van der Vorst. Parallel Numerical Linear Algebra. *Acta Numerica*, 2:111–197, 1993.
- [16] J. Dongarra, P. Beckman, T. Moore, P. Aerts, G. Aloisio, J. Andre, D. Barkai, J. Berthou, T. Boku, B. Braunschweig, et al. The international exascale software project roadmap. *International Journal of High Performance Computing Applications*, 25(1):3–60, 2011.
- [17] J. Dongarra and M.A. Heroux. Toward a new metric for ranking high performance computing systems. *Sandia National Laboratories Technical Report, SAND2013-4744*, 312, 2013.
- [18] J. Dongarra, M.A. Heroux, and P. Luszczek. HPCG benchmark: a new metric for ranking high performance computing systems. *University of Tennessee, Electrical Engineering and Computer Science Department, Technical Report UT-EECS-15-736*, 2015.
- [19] P.R. Eller and W. Gropp. Scalable non-blocking preconditioned Conjugate Gradient methods. In *SC16: International Conference for High Performance Computing, Networking, Storage and Analysis*, pages 204–215. IEEE, 2016.
- [20] J. Erhel. A parallel GMRES version for general sparse matrices. *Electronic Transactions on Numerical Analysis*, 3(12):160–176, 1995.
- [21] V. Faber, J. Liesen, and P. Tichý. On Chebyshev polynomials of matrices. *SIAM Journal on Matrix Analysis and Applications*, 31(4):2205–2221, 2010.
- [22] S.H. Fuller and L.I. Millett (Eds.) National Research Council of the National Academies. *The Future of Computing Performance: Game Over or Next Level?* National Academies Press, 2011.
- [23] T. Gergelits and Z. Strakoš. Composite convergence bounds based on Chebyshev polynomials and finite precision Conjugate Gradient computations. *Numerical Algorithms*, 65(4):759–782, 2014.
- [24] P. Ghysels, T.J. Ashby, K. Meerbergen, and W. Vanroose. Hiding global communication latency in the GMRES algorithm on massively parallel machines. *SIAM Journal on Scientific Computing*, 35(1):C48–C71, 2013.
- [25] P. Ghysels and W. Vanroose. Hiding global synchronization latency in the preconditioned Conjugate Gradient algorithm. *Parallel Computing*, 40(7):224–238, 2014.
- [26] A. Greenbaum. Behavior of slightly perturbed Lanczos and Conjugate-Gradient recurrences. *Linear Algebra and its Applications*, 113:7–63, 1989.
- [27] A. Greenbaum. Estimating the attainable accuracy of recursively computed residual methods. *SIAM Journal on Matrix Analysis and Applications*, 18(3):535–551, 1997.
- [28] A. Greenbaum. *Iterative methods for solving linear systems*. SIAM, 1997.
- [29] A. Greenbaum and Z. Strakoš. Predicting the behavior of finite precision Lanczos and Conjugate Gradient computations. *SIAM Journal on Matrix Analysis and Applications*, 13(1):121–137, 1992.
- [30] A. Greenbaum and L.N. Trefethen. GMRES/CR and Arnoldi/Lanczos as matrix approximation problems. *SIAM Journal on Scientific Computing*, 15(2):359–368, 1994.
- [31] L. Grigori, S. Moufawad, and F. Nataf. Enlarged Krylov subspace Conjugate Gradient methods for reducing communication. *SIAM Journal on Matrix Analysis and Applications*, 37(2):744–773, 2016.
- [32] M.H. Gutknecht and Z. Strakoš. Accuracy of two three-term and three two-term recurrences for Krylov space

- solvers. *SIAM Journal on Matrix Analysis and Applications*, 22(1):213–229, 2000.
- [33] M.R. Hestenes and E. Stiefel. Methods of Conjugate Gradients for solving linear systems. *Journal of Research of the National Bureau of Standards*, 14(6), 1952.
- [34] M. Hoemmen. *Communication-avoiding Krylov subspace methods*, PhD dissertation. EECS Department, University of California, Berkeley, 2010.
- [35] D. Imberti and J. Erhel. Varying the  $s$  in your  $s$ -step GMRES. *Electronic Transactions on Numerical Analysis*, 47:206–230, 2017.
- [36] J. Liesen and Z. Strakoš. *Krylov Subspace Methods: Principles and Analysis*. Oxford University Press, 2012.
- [37] L.C. McInnes, B. Smith, H. Zhang, and R.T. Mills. Hierarchical Krylov and nested Krylov methods for extreme-scale computing. *Parallel Computing*, 40(1):17–31, 2014.
- [38] G. Meurant. Multitasking the Conjugate Gradient method on the CRAY X-MP/48. *Parallel Computing*, 5(3):267–280, 1987.
- [39] G. Meurant. *Computer solution of large linear systems*, volume 28. Elsevier, 1999.
- [40] G. Meurant and Z. Strakoš. The Lanczos and Conjugate Gradient algorithms in finite precision arithmetic. *Acta Numerica*, 15:471–542, 2006.
- [41] C.C. Paige and M.A. Saunders. Solution of sparse indefinite systems of linear equations. *SIAM Journal on Numerical Analysis*, 12(4):617–629, 1975.
- [42] Y. Saad. Practical use of some Krylov subspace methods for solving indefinite and nonsymmetric linear systems. *SIAM Journal on Scientific and Statistical Computing*, 5(1):203–228, 1984.
- [43] Y. Saad. *Iterative methods for sparse linear systems*. SIAM, 2003.
- [44] P. Sanan, S.M. Schnepp, and D.A. May. Pipelined, Flexible Krylov Subspace Methods. *SIAM Journal on Scientific Computing*, 38(5):C441–C470, 2016.
- [45] Z. Strakoš. Effectivity and optimizing of algorithms and programs on the host-computer/array-processor system. *Parallel Computing*, 4(2):189–207, 1987.
- [46] Z. Strakoš and P. Tichý. On error estimation in the Conjugate Gradient method and why it works in finite precision computations. *Electronic Transactions on Numerical Analysis*, 13:56–80, 2002.
- [47] Z. Strakoš and P. Tichý. Error estimation in preconditioned Conjugate Gradients. *BIT Numerical Mathematics*, 45(4):789–817, 2005.
- [48] H.A. Van der Vorst. *Iterative Krylov methods for large linear systems*, volume 13. Cambridge University Press, 2003.
- [49] I. Yamazaki, M. Hoemmen, P. Luszczek, and J. Dongarra. Improving performance of GMRES by reducing communication and pipelining global collectives. In *Parallel and Distributed Processing Symposium Workshops (IPDPSW), 2017 IEEE International*, pages 1118–1127. IEEE, 2017.
- [50] S. Zhuang and M. Casas. Iteration-Fusing Conjugate Gradient. In *Proceedings of the International Conference on Supercomputing*, pages 21–30. ACM, 2017.



### Appendix B. A practical basis storage framework using sliding windows.

Since in each iteration  $i$  of  $p(l)$ -CG, Alg. 2, only the last  $l+1$  vectors  $z_{i-l+1}, \dots, z_{i+1}$  are required, these vectors are stored in a sliding window of  $l+1$  vectors. We denote this window by  $\vec{Z}_i$ , where the index  $i$  indicates the *current iteration*. Note that this is in contrast to the indexing for the basis  $Z_i := [z_0, \dots, z_{i-1}]$ , where the index  $i$  denotes the *number of vectors* in the basis. The sliding window  $\vec{Z}_i$  is defined as

$$\vec{Z}_i = [\vec{Z}_i(0), \vec{Z}_i(1), \dots, \vec{Z}_i(l)] = \begin{cases} [ \dots, z_{i+1}, \dots, z_0], & 0 \leq i < l, \\ [z_{i+1}, z_i, \dots, z_{i-l+1}], & i \geq l. \end{cases}$$

Vectors  $z_j$  in the sliding window are listed from highest to lowest index, i.e. for  $i \geq l$  the vector in the first position in the sliding window is  $z_{i+1}$ , and the vector in the last position is  $z_{i-l+1}$ , see also Fig. 2. A particular vector  $z_j$  with  $\max(0, i-l+1) \leq j \leq i+1$  can be accessed from  $\vec{Z}_i$  as follows:

$$z_j = \begin{cases} \vec{Z}_i(l-j), & 0 \leq i < l, \\ \vec{Z}_i(i-j+1), & i \geq l. \end{cases}$$

For iterations  $0 \leq i \leq l-1$  the window  $\vec{Z}_i$  is being filled up by simply adding vectors as follows:

$$\vec{Z}_0 = [ \dots, z_1, z_0], \quad \vec{Z}_1 = [ \dots, z_2, z_1, z_0], \quad \dots, \quad \vec{Z}_{l-1} = [z_l, \dots, z_3, z_2, z_1, z_0].$$

From iteration  $i = l$  onward the window effectively starts to *slide*: the most recently computed basis vector  $z_{i+1}$  is written to position  $\vec{Z}_i(0)$ , and the vectors  $z_i, \dots, z_{i-l}$  from the previous window  $\vec{Z}_{i-1}$  are all moved one space to a higher position in the window  $\vec{Z}_i$ . As a result of this procedure the vector  $z_{i-l}$  is dropped from the window  $\vec{Z}_i$ . Hence we obtain for  $i \geq l$ :

$$\vec{Z}_l = [z_{l+1}, \dots, z_3, z_2, z_1], \quad \vec{Z}_{l+1} = [z_{l+2}, \dots, z_4, z_3, z_2], \quad \dots, \quad \vec{Z}_i = [z_{i+1}, z_i, \dots, z_{i-l+1}].$$

The procedure for filling and maintaining the sliding window  $\vec{Z}_i$  is illustrated in Fig. 12 (left) for pipeline length  $l = 2$ . In this case the window  $\vec{Z}_i$  contains  $l+1 = 3$  vectors in each iteration  $i \geq l-1$ .

Similarly to the auxiliary basis  $Z_{i+2}$ , each  $p(l)$ -CG iteration  $i$  uses the last  $2l+1$  basis vectors  $v_{i-3l+1}, \dots, v_{i-l+1} \in V_{i-l+2}$  to update the solution, see Alg. 2. These basis vectors are stored using a second sliding window  $\vec{V}_i$  consisting of  $2l+1$  vectors, where again the index  $i$  refers to the iteration. The window  $\vec{V}_i$  is defined similarly to the window  $\vec{Z}_i$  above, i.e.:

$$\vec{V}_i = [\vec{V}_i(0), \vec{V}_i(1), \dots, \vec{V}_i(2l)] = \begin{cases} [ \dots, v_0], & 0 \leq i < l, \\ [ \dots, v_{i-l+1}, \dots, v_0], & l \leq i < 3l, \\ [v_{i-l+1}, v_{i-l}, \dots, v_{i-3l+1}], & i \geq 3l, \end{cases}$$

and a particular vector  $v_j$  with  $\max(0, i-3l+1) \leq j \leq i-l+1$  can be accessed from  $\vec{V}_i$  as follows:

$$v_j = \begin{cases} \vec{V}_i(2l-j), & l \leq i < 3l, \\ \vec{V}_i(i-l-j+1), & i \geq 3l. \end{cases}$$

The window  $\vec{V}_i$  for the basis  $V_{i-l+2}$  only starts to get filled once the window  $\vec{Z}_i$  for the auxiliary basis  $Z_{i+2}$  has been completely filled. Indeed, for iterations 0 up to  $l-1$  no vectors  $v_{i-l+1}$  are

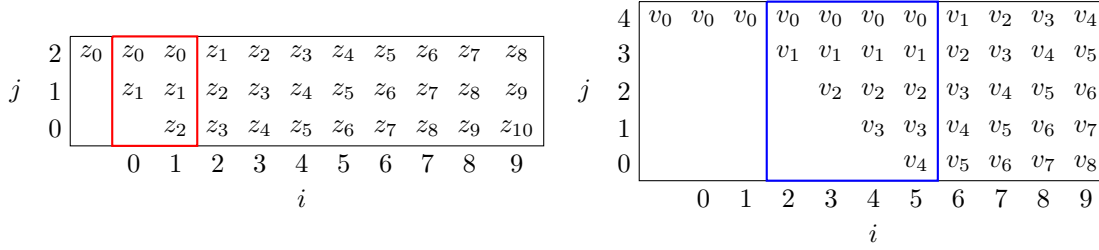


FIG. 12. Schematic representation of the sliding storage windows  $\vec{Z}_i(j)$  and  $\vec{V}_i(j)$  in the first 10 iterations of Alg. 2 for pipeline length  $l = 2$ . **Left:** red box indicates the initial filling of the window  $\vec{Z}_i$  in iterations 0 up to  $l - 1$ . The window  $\vec{Z}_i$  effectively starts sliding from iteration  $l$  onward. **Right:** blue box indicates the initial filling of the window  $\vec{V}_i$  in iterations  $l$  up to  $3l - 1$ , after the window  $\vec{Z}_i$  has been completely filled (see left). The window  $\vec{V}_i$  starts sliding from iteration  $3l$  onward.

computed in Alg. 2, i.e.:

$$\vec{V}_0 = [ \dots, \dots, v_0 ], \quad \vec{V}_1 = [ \dots, \dots, v_0 ], \quad \dots, \quad \vec{V}_{l-1} = [ \dots, \dots, v_0 ].$$

In iterations  $l$  up to  $3l - 1$  the window  $\vec{V}_i$  is gradually filled by adding one vector  $v_{i-l+1}$  in each iteration  $i$ :

$$\vec{V}_l = [ \dots, \dots, v_1, v_0 ], \quad \vec{V}_{l+1} = [ \dots, \dots, v_2, v_1, v_0 ], \quad \dots, \quad \vec{V}_{3l-1} = [ v_{2l}, \dots, v_3, v_2, v_1, v_0 ].$$

The window  $\vec{V}_i$  is completely filled for the first time in iteration  $3l - 1$ . Consequently,  $\vec{V}_i$  effectively starts to slide from iteration  $3l$  onwards, i.e.:

$$\vec{V}_{3l} = [ v_{2l+1}, \dots, v_3, v_2, v_1 ], \quad \vec{V}_{3l+1} = [ v_{2l+2}, \dots, v_4, v_3, v_2 ], \quad \dots, \quad \vec{V}_i = [ v_{i-l+1}, v_{i-l}, \dots, v_{i-3l+1} ].$$

Fig. 12 (right) illustrates the above procedure by showing a schematic overview of the sliding window  $\vec{V}_i$  in the first iterations of Alg. 2 for pipeline length  $l = 2$ . Notice how in iteration  $i$  the basis  $V_{i-l+2}$ , characterized by the sliding window  $\vec{V}_i$ , contains the last updated basis vector  $v_{i-l+1} = v_{i-1}$ . The basis  $V_{i-l+2}$  thus runs  $l$  vectors behind compared to the auxiliary basis  $Z_{i+2}$  represented by the sliding window  $\vec{Z}_i$ , which contains the most recent auxiliary basis vector  $z_{i+1}$ , see Fig. 12 (left).

The concept of sliding windows can analogously be applied to the basis  $\hat{Z}_i$  in the preconditioned version of the  $l$ -length pipelined CG method. The sliding window for the preconditioned auxiliary basis  $\hat{Z}_{i+2}$  is however limited to the last three vectors  $\hat{z}_{i-1}$ ,  $\hat{z}_i$  and  $\hat{z}_{i+1}$ , since only these vectors need to be stored in iteration  $i$  of the algorithm, see Remark 14.

The sliding of the window can easily be implemented in practice by re-addressing the pointers to the array elements in the windows  $\vec{Z}_i$  and  $\vec{V}_i$ . For example, the C-code snippet

```
Vec *Z_VEC, temp;
temp = Z_VEC[l];
for(i = l; i > 0; i--) Z_VEC[i] = Z_VEC[i-1];
Z_VEC[0] = temp;
MatMult(A, Z_VEC[1], Z_VEC[0]);
```

illustrates the sliding of the window  $\vec{Z}_i$  in iteration  $i \geq l$ , where  $Z\_VEC$  is an array of pointers to the vectors in  $\vec{Z}_i$ . The pointers are cycled such that  $z_{i+1} = Az_i$  can be added to the window as  $\vec{Z}_i(0)$ .

### Appendix C. Summary of rounding error analysis for classic CG and p-CG.

We provide a brief overview of the analysis of local rounding errors in classic CG and p-CG, which was performed in detail in [12] and the related work [6]. This section is intended as an easy reference to compare the numerical analysis of the p( $l$ )-CG method to the existing CG and p-CG methods.

**C.1. Local rounding error behavior in finite precision classic CG.** Consider the propagation of local rounding errors by the recurrence relations of classic CG, Alg. 4, given by expression (33). By introducing the matrix notation  $\bar{\mathbf{R}}_{j+1} - \bar{R}_{j+1} = [\bar{\mathbf{r}}_0 - \bar{r}_0, \dots, \bar{\mathbf{r}}_j - \bar{r}_j]$  for the residual gaps in the first  $j + 1$  iterations and by analogously defining  $\Theta_j^{\bar{x}} = [0, -\xi_1^{\bar{x}}, \dots, -\xi_{j-1}^{\bar{x}}]$  and  $\Theta_j^{\bar{r}} = [f_0, -\xi_1^{\bar{r}}, \dots, -\xi_{j-1}^{\bar{r}}]$  for the local rounding errors, expression (33) can be formulated as

$$\bar{\mathbf{R}}_{j+1} - \bar{R}_{j+1} = (A\Theta_{j+1}^{\bar{x}} + \Theta_{j+1}^{\bar{r}}) E_{j+1},$$

where  $E_{j+1}$  is a  $(j + 1) \times (j + 1)$  upper triangular matrix of ones. Since all entries of  $E_{j+1}$  are one, local rounding errors are merely accumulated (not amplified) in the classic CG algorithm.

**C.2. Local rounding error behavior in finite precision p-CG.** The pipelined p-CG method proposed in [25], see Alg. 5, uses additional recurrence relations for auxiliary vector quantities defined as  $w_j := Ar_j$ ,  $s_j := Ap_j$  and  $z_j := As_j$ . The coupling between these recursively defined variables may cause local rounding error amplification. In finite precision p-CG the following recurrence relations are computed:

$$\begin{aligned} \bar{x}_{j+1} &= \bar{x}_j + \bar{\alpha}_j \bar{p}_j + \xi_{j+1}^{\bar{x}}, & \bar{w}_{j+1} &= \bar{w}_j - \bar{\alpha}_j \bar{z}_j + \xi_{j+1}^{\bar{w}}, & \bar{r}_{j+1} &= \bar{r}_j - \bar{\alpha}_j \bar{s}_j + \xi_{j+1}^{\bar{r}}, \\ \bar{s}_j &= \bar{w}_j + \bar{\beta}_j \bar{s}_{j-1} + \xi_j^{\bar{s}}, & \bar{p}_j &= \bar{r}_j + \bar{\beta}_j \bar{p}_{j-1} + \xi_j^{\bar{p}}, & \bar{z}_j &= A\bar{w}_j + \bar{\beta}_j \bar{z}_{j-1} + \xi_j^{\bar{z}}. \end{aligned}$$

The respective bounds for the local rounding errors  $\xi_k^{\bar{x}}, \xi_k^{\bar{r}}, \xi_k^{\bar{p}}, \xi_k^{\bar{s}}, \xi_k^{\bar{w}}$  and  $\xi_k^{\bar{z}}$  in these recurrence relations can be found in [12], where it is also shown that the residual gap  $(b - A\bar{x}_j) - \bar{r}_j$  is coupled to the gaps  $A\bar{p}_j - \bar{s}_j$ ,  $A\bar{r}_j - \bar{w}_j$  and  $A\bar{s}_j - \bar{z}_j$  on the auxiliary variables in p-CG.

Let  $B = [b, b, \dots, b]$ ,  $\bar{X}_{j+1} = [\bar{x}_0, \bar{x}_1, \dots, \bar{x}_j]$  and  $\bar{P}_{j+1} = [\bar{p}_0, \bar{p}_1, \dots, \bar{p}_j]$ . Writing the gaps defined in [12] (Section 2.3) in matrix notation as  $\bar{\mathbf{R}}_{j+1} - \bar{R}_{j+1}$ ,  $\bar{\mathbf{S}}_{j+1} - \bar{S}_{j+1}$ ,  $\bar{\mathbf{W}}_{j+1} - \bar{W}_{j+1}$ ,  $\bar{\mathbf{Z}}_{j+1} - \bar{Z}_{j+1}$  with actual variables that are defined as  $\bar{\mathbf{R}}_{j+1} = B - A\bar{X}_{j+1}$ ,  $\bar{\mathbf{S}}_{j+1} = A\bar{P}_{j+1}$ ,  $\bar{\mathbf{W}}_{j+1} = A\bar{R}_{j+1}$  and  $\bar{\mathbf{Z}}_{j+1} = A\bar{S}_{j+1}$ , and using the expressions for the local rounding errors on the auxiliary variables:  $\Theta_j^{\bar{x}} = -[0, \xi_1^{\bar{x}}, \dots, \xi_{j-1}^{\bar{x}}]$ ,  $\Theta_j^{\bar{r}} = [f_0, -\xi_1^{\bar{r}}, \dots, -\xi_{j-1}^{\bar{r}}]$ ,  $\Theta_j^{\bar{p}} = [0, \xi_1^{\bar{p}}, \dots, \xi_{j-1}^{\bar{p}}]$ ,  $\Theta_j^{\bar{s}} = [g_0, -\xi_1^{\bar{s}}, \dots, -\xi_{j-1}^{\bar{s}}]$ ,  $\Theta_j^{\bar{w}} = [0, \xi_1^{\bar{w}}, \dots, \xi_{j-1}^{\bar{w}}]$ ,  $\Theta_j^{\bar{z}} = [h_0, -\xi_1^{\bar{z}}, \dots, -\xi_{j-1}^{\bar{z}}]$ , the following matrix expressions for the gaps in p-CG are obtained:

$$\begin{aligned} \bar{\mathbf{R}}_{j+1} - \bar{R}_{j+1} &= (A\Theta_{j+1}^{\bar{x}} + \Theta_{j+1}^{\bar{r}}) E_{j+1} + (\bar{\mathbf{S}}_{j+1} - \bar{S}_{j+1}) \bar{\mathcal{A}}_{j+1}, \\ \bar{\mathbf{S}}_{j+1} - \bar{S}_{j+1} &= (A\Theta_{j+1}^{\bar{p}} + \Theta_{j+1}^{\bar{s}}) \bar{\mathcal{B}}_{j+1}^{-1} + (\bar{\mathbf{W}}_{j+1} - \bar{W}_{j+1}) \bar{\mathcal{B}}_{j+1}^{-1}, \\ \bar{\mathbf{W}}_{j+1} - \bar{W}_{j+1} &= (A\Theta_{j+1}^{\bar{w}} + \Theta_{j+1}^{\bar{z}}) E_{j+1} + (\bar{\mathbf{Z}}_{j+1} - \bar{Z}_{j+1}) \bar{\mathcal{A}}_{j+1}, \\ \bar{\mathbf{Z}}_{j+1} - \bar{Z}_{j+1} &= (A\Theta_{j+1}^{\bar{z}} + \Theta_{j+1}^{\bar{z}}) \bar{\mathcal{B}}_{j+1}^{-1}. \end{aligned}$$

By substituting these expressions we obtain the following expression for the residual gaps in p-CG:

$$\begin{aligned} \bar{\mathbf{R}}_{j+1} - \bar{R}_{j+1} &= (A\Theta_{j+1}^{\bar{x}} + \Theta_{j+1}^{\bar{r}}) E_{j+1} + (A\Theta_{j+1}^{\bar{p}} + \Theta_{j+1}^{\bar{s}}) \bar{\mathcal{B}}_{j+1}^{-1} \bar{\mathcal{A}}_{j+1} + \dots \\ &\quad + (A\Theta_{j+1}^{\bar{w}} + \Theta_{j+1}^{\bar{z}}) E_{j+1} \bar{\mathcal{B}}_{j+1}^{-1} \bar{\mathcal{A}}_{j+1} + (A\Theta_{j+1}^{\bar{z}} + \Theta_{j+1}^{\bar{z}}) \bar{\mathcal{B}}_{j+1}^{-1} \bar{\mathcal{A}}_{j+1} \bar{\mathcal{B}}_{j+1}^{-1} \bar{\mathcal{A}}_{j+1}, \end{aligned}$$

where

$$\bar{\mathcal{A}}_{j+1} = - \begin{pmatrix} 0 & \bar{\alpha}_0 & \bar{\alpha}_0 & \cdots & \bar{\alpha}_0 \\ & 0 & \bar{\alpha}_1 & \cdots & \bar{\alpha}_1 \\ & & \ddots & & \vdots \\ & & & 0 & \bar{\alpha}_{j-1} \\ & & & & 0 \end{pmatrix}, \quad \bar{\mathcal{B}}_{j+1}^{-1} = \begin{pmatrix} 1 & \bar{\beta}_1 & \bar{\beta}_1\bar{\beta}_2 & \cdots & \bar{\beta}_1\bar{\beta}_2\cdots\bar{\beta}_j \\ & 1 & \bar{\beta}_2 & \ddots & \bar{\beta}_2\cdots\bar{\beta}_j \\ & & \ddots & \ddots & \vdots \\ & & & \ddots & \bar{\beta}_j \\ & & & & 1 \end{pmatrix}.$$

Hence, the entries of the coefficient matrices  $\bar{\mathcal{B}}_{j+1}^{-1}$  and  $\bar{\mathcal{A}}_{j+1}$  determine the propagation of the local rounding errors in p-CG. The entries of  $\bar{\mathcal{B}}_{j+1}^{-1}$  consist of a product of the scalar coefficients  $\bar{\beta}_j$ . In exact arithmetic these coefficients equal  $\beta_j = \|r_j\|^2/\|r_{j-1}\|^2$ , such that

$$\beta_i \beta_{i+1} \cdots \beta_j = \frac{\|r_i\|^2}{\|r_{i-1}\|^2} \frac{\|r_{i+1}\|^2}{\|r_i\|^2} \cdots \frac{\|r_j\|^2}{\|r_{j-1}\|^2} = \frac{\|r_j\|^2}{\|r_{i-1}\|^2}, \quad i \leq j.$$

Since the residual norm in CG is not guaranteed to decrease monotonically, the factor  $\|r_j\|^2/\|r_{i-1}\|^2$  may for some  $i \leq j$  be much larger than one. A similar argument may be used in the finite precision framework to derive that some entries of  $\bar{\mathcal{B}}_{j+1}^{-1}$  may be significantly larger than one, and may hence (possibly dramatically) amplify the corresponding local rounding errors. This behavior is illustrated in Section 5 by Fig. 6, 9, 10 and 11, where the p-CG residual norm typically stagnates at a reduced maximal attainable accuracy level compared to classic CG.

---

**Algorithm 4** Conjugate Gradient method (CG) **Input:**  $A, b, x_0, m, \tau$

---

```

1:  $r_0 := b - Ax_0$ ;
2:  $p_0 := r_0$ ;
3: for  $i = 0, \dots, m$  do
4:    $s_i := Ap_i$ ;
5:    $\alpha_i := (r_i, r_i) / (s_i, p_i)$ ;
6:   end if
7:    $x_{i+1} := x_i + \alpha_i p_i$ ;
8:    $r_{i+1} := r_i - \alpha_i s_i$ ;
9:    $\beta_{i+1} := (r_{i+1}, r_{i+1}) / (r_i, r_i)$ ;
10:   $p_{i+1} := r_{i+1} + \beta_{i+1} p_i$ ;
11: end for
    
```

---



---

**Algorithm 5** Pipelined Conjugate Gradient method (p-CG) **Input:**  $A, b, x_0, m, \tau$

---

```

1:  $r_0 := b - Ax_0$ ;
2:  $w_0 := Ar_0$ ;
3: for  $i = 0, \dots, m$  do
4:    $\gamma_i := (r_i, r_i)$ ;
5:    $\delta_i := (w_i, r_i)$ ;
6:    $v_i := Aw_i$ ;
7:   end if
8:   if  $i > 0$  then
9:      $\beta_i := \gamma_i / \gamma_{i-1}$ ;
10:     $\alpha_i := (\delta_i / \gamma_i - \beta_i / \alpha_{i-1})^{-1}$ ;
11:   else
12:      $\beta_i := 0$ ;
13:      $\alpha_i := \gamma_i / \delta_i$ ;
14:   end if
15:    $z_i := v_i + \beta_i z_{i-1}$ ;
16:    $s_i := w_i + \beta_i s_{i-1}$ ;
17:    $p_i := r_i + \beta_i p_{i-1}$ ;
18:    $x_{i+1} := x_i + \alpha_i p_i$ ;
19:    $r_{i+1} := r_i - \alpha_i s_i$ ;
20:    $w_{i+1} := w_i - \alpha_i z_i$ ;
21: end for
    
```

---

Appendix D. Supplementary numerical results on maximal attainable accuracy.

Matrix	Prec	$\kappa(A)$	$n$	$\#mnz$	$\ b\ _2$	CG	p-CG	p(1)-CG	p(2)-CG	p(3)-CG	p(4)-CG	p(5)-CG	iter
bosstk14	JAC	1.3e+10	1806	63,454	2.1e+09	8.2e-16	2.3e-12	2.3e-16	5.9e-13	7.3e-12	3.0e-12	1.2e-10	700
bosstk15	JAC	8.0e+09	3948	117,816	4.3e+08	3.7e-15	2.4e-12	3.2e-14	2.2e-06	3.5e-06	2.1e-06	2.0e-06	780
bosstk16	JAC	65	4884	290,378	1.5e+08	3.7e-15	6.3e-12	1.1e-14	8.5e-12	5.6e-11	1.5e-10	8.5e-11	300
bosstk17	JAC	65	10,974	428,650	9.0e+07	1.5e-14	4.4e-09	1.4e-04	2.1e-06	3.5e-06	1.8e-06	5.3e-06	3600
bosstk18	JAC	65	11,948	149,090	2.6e+09	2.3e-15	1.2e-10	5.4e-11	3.9e-13	1.1e-12	3.0e-11	1.6e-11	2400
bosstk27	JAC	7.7e+04	1224	56,126	1.1e+05	3.6e-15	1.8e-11	1.2e-14	2.3e-11	9.2e-09	1.1e-08	7.7e-09	350
gr_30_30	-	3.8e+02	900	7744	1.1e+00	8.3e-14	3.1e-13	8.9e-15	1.6e-14	1.9e-15	1.9e-15	2.1e-15	60
nos1	*ICG	2.5e+07	237	1017	5.7e+07	1.1e-14	4.2e-10	4.3e-11	1.3e-05	7.9e-05	6.0e-03	6.6e-05	350
nos2	*ICG	6.3e+09	957	4137	1.8e+09	8.3e-14	1.0e-07	4.4e-06	1.4e-05	1.4e-05	9.7e-06	1.0e-05	3180
nos3	ICG	7.3e+04	960	15,844	1.0e+01	9.6e-15	2.4e-12	2.4e-14	4.1e-14	2.4e-14	9.8e-15	5.4e-13	65
nos4	ICG	2.7e+03	100	594	5.2e-02	1.9e-15	3.5e-14	7.2e-16	7.6e-16	3.6e-15	4.0e-15	6.0e-15	33
nos5	ICG	2.9e+04	468	5172	2.8e+05	3.1e-16	6.7e-14	2.8e-16	1.8e-16	2.3e-16	6.8e-16	2.7e-16	63
nos6	ICG	8.0e+06	675	3255	8.6e+04	5.0e-15	4.1e-11	4.8e-14	6.1e-09	5.0e-08	4.3e-08	2.4e-08	34
nos7	ICG	4.1e+09	729	4617	8.6e-03	3.1e-08	1.1e-07	5.4e-08	9.9e-08	1.6e-07	2.7e-05	5.9e-04	31
s1rmq4m1	ICG	1.8e+06	5489	262,411	1.5e+04	4.7e-15	5.5e-12	8.5e-15	8.1e-14	4.9e-15	3.1e-15	2.3e-14	135
s1rm3m1	ICG	2.5e+06	5489	217,651	1.5e+04	8.9e-15	4.1e-11	3.0e-15	2.7e-13	3.2e-13	2.7e-12	4.0e-13	245
s2rmq4m1	*ICG	1.8e+08	5489	263,351	1.5e+03	7.1e-15	3.0e-10	3.4e-13	6.0e-11	6.8e-06	1.4e-05	1.1e-05	370
s2rm3m1	ICG	2.5e+08	5489	217,681	1.5e+03	2.3e-14	7.4e-10	1.2e-12	4.9e-12	9.6e-06	7.1e-06	6.9e-06	265
s3rmq4m1	*ICG	1.8e+10	5489	262,943	1.5e+02	1.5e-14	2.9e-08	1.9e-06	1.8e-06	2.5e-05	9.5e-07	3.9e-07	1650
s3rm3m1	*ICG	2.5e+10	5489	217,669	1.5e+02	2.9e-14	1.0e-07	2.3e-09	2.3e-07	3.5e-07	4.9e-07	5.2e-07	2282
s3rm3m3	*ICG	2.4e+10	5357	207,123	1.3e+02	3.2e-14	2.4e-07	1.4e-07	1.7e-07	4.8e-06	4.9e-06	1.6e-05	2862

TABLE 2

A random selection of real, non-diagonal and symmetric positive definite matrices from Matrix Market, listed with their respective condition number  $\kappa(A)$ , number of rows/columns  $n$  and total number of nonzeros  $\#mnz$ . A linear system with right-hand side  $b = A\tilde{x}$  where  $\tilde{x}_i = 1/\sqrt{n}$  is solved with each matrix. The initial guess is all-zero  $\tilde{x}_0 = 0$ . Preconditioners Jacobi (JAC), Incomplete Cholesky factorization (ICG) and compensated Incomplete Cholesky with global diagonal shift (ICG\*) are included where required. For each problem the number of iterations (and thus the number of SPNV and preconditioner applications) performed is fixed for all methods. The number of iterations performed is fixed per problem for all methods and is based on classic CG reaching maximal attainable accuracy (stagnation point). The relative residuals  $\|b - A\tilde{x}_i\|_2/\|b\|_2$  are shown for all methods. Pipelined methods generally reach a lower precision compared to classic CG for the same number of SPNVs (iterations) and the loss of attainable accuracy is more pronounced for longer pipelines, cf. Section 4.